IFITM proteins promote SARS-CoV-2 infection of human lung cells

Caterina Prelli Bozzo[1], Rayhane Nchioua[1], Meta Volcic[1], Lukas Wettstein[1], Tatjana Weil[1], Jana Krüger[2], Sandra Heller[2], Carina Conzelmann[1], Janis Müller[1], Rüdiger Gross[1], Fabian Zech[1], Desiree Schütz[1], Lennart Koepke[1], Christina M Stuerzel[1], Christiane Schüler[3], Saskia Stenzel[3], Elisabeth Braun[1], Johanna Weiß[1], Daniel Sauter[1], Jan Münch[1], Steffen Stenger[4], Kei Sato[5], Alexander Kleger[2], Christine Goffinet[3], Konstantin M.J. Sparrer[1*] and Frank Kirchhoff[1*]

[1] Institute for Molecular Virology
Ulm University Medical Centre
89081 Ulm, Germany

[2] Department of Internal Medicine I
Ulm University Medical Centre
89081 Ulm, Germany

[3] Institute of Virology
Campus Charité Mitte
Charité - Universitätsmedizin Berlin
10117 Berlin, Germany

[4] Institute of Medical Microbiology and Hygiene
Ulm University Medical Centre
89081 Ulm, Germany

[5] Laboratory of Systems Virology
Institute for Frontier Life and Medical Sciences
Kyoto University, Kyoto, Japan.

* Correspondence: konstantin.sparrer@uni-ulm.de or Frank.Kirchhoff@uni-ulm.de

Running title: IFITMs promote SARS-CoV-2 infection

KEYWORDS: SARS-CoV-2, Interferon-induced transmembrane proteins, spike glycoproteins, human lung cells, viral entry cofactors

ABSTRACT

Interferon-induced transmembrane proteins (IFITMs 1, 2 and 3) restrict numerous viral pathogens and are thought to prevent infection by severe acute respiratory syndrome coronaviruses (SARS-CoVs). However, most evidence comes from single-round pseudoparticle infection of cells artificially overexpressing IFITMs. Here, we confirmed that overexpression of IFITMs blocks pseudoparticle infections mediated by the Spike proteins of β-coronaviruses including pandemic SARS-CoV-2. In striking contrast, however, endogenous IFITM expression promoted genuine SARS-CoV-2 infection in human lung cells both in the presence and absence of interferon. IFITM2 was most critical for efficient entry of SARS-CoV-2 and enhanced virus production from Calu-3 cells by several orders of magnitude. IFITMs are expressed and further induced by interferons in the lung representing the primary site of SARS-CoV-2 infection as well as in other relevant tissues. Our finding that IFITMs enhance SARS-CoV-2 infection under conditions approximating the *in vivo* situation shows that they may promote viral invasion during COVID-19.

HIGHLIGHTS

- **Overexpression of IFITM1, 2 and 3 restricts SARS-CoV-2 infection**
- **Endogenous IFITM1, 2 and 3 boost SARS-CoV-2 infection of human lung cells**
- **IFITM2 is critical for efficient entry of SARS-CoV-2 in Calu-3 cells**

INTRODUCTION

SARS-CoV-2 is the cause of pandemic Coronavirus disease 2019 (COVID-19). Originating from China in late 2019, the virus spread rapidly, causing a serious threat to human health worldwide, impacting our daily lives and global economy (Zhou et al., 2020). Most countries have enacted protective measures to curb the pandemic. Yet transmission rates remain high and the virus has infected more than 21 million people around the globe (https://coronavirus.jhu.edu/map.html). While SARS-CoV-2 spreads more efficiently than SARS-CoV and MERS-CoV, the previously emerging causative agents of severe acute respiratory syndromes (SARS), it shows a lower case-fatality rate (~2 to 5%), compared to ~10% and almost 40%, respectively (Bermingham et al., 2012; Ksiazek et al., 2003). It has been reported that SARS-CoV-2 is more susceptible to inhibition by interferons (IFNs) than SARS-CoV (Mantlo et al., 2020) and treatment with IFNs is considered a therapeutic option to treat COVID-19 (Sallard et al., 2020). However, IFNs may also exert detrimental effects and contribute to tissues damage and severe COVID-19 (Major et al., 2020). Finally, IFNs and other pro-inflammatory cytokines induce hundreds of cellular factors (Sparrer and Gack, 2015) whose effects on SARS-CoV-2 infection are currently poorly understood (Sa Ribero et al., 2020).

Here, we focused on innate immune effectors that may target the first essential step of SARS-CoV-2 replication: entry into its target cells. To enter host cells, the receptor-binding-domain of the SARS-CoV-2 Spike (S) protein recognizes the cell surface receptor angiotensin-converting enzyme 2 (ACE2) (Hoffmann et al., 2020a; Letko et al., 2020). To undergo the required conformational changes for fusion, the S protein is proteolytically cleaved into S1 and S2 by TMPRSS2 on the plasma membrane or by lysosomal proteases (Hoffmann et al., 2020b, 2020a; Matsuyama et al., 2010). A prominent family of IFN stimulated genes (ISGs) known to inhibit fusion between the viral and cellular membranes are interferon-inducible transmembrane (IFITM) proteins (Diamond and Farzan, 2013; Zhao et al., 2019). These trans-membrane proteins restrict entry of many enveloped viruses including Influenza A viruses, Flaviviruses, Rhabdoviruses, Bunyaviruses and human

immunodeficiency viruses (Diamond and Farzan, 2013; Huang et al., 2011). It has also been shown that overexpression of IFITM proteins inhibits transduction by viral particles pseudotyped with the S proteins of SARS- and MERS-CoVs (Huang et al., 2011; Wrensch et al., 2014). Thus, it is thought that IFITMs restrict replication of pathogenic SARS coronaviruses (Bailey et al., 2014). Notably, previous studies have reported that IFITMs can enhance infection with the non-epidemic human Coronavirus OC43 (Huang et al., 2011; Wrensch et al., 2014; Zhao et al., 2014). Furthermore, mutants of IFITM3 were reported to promote the infection of many Coronaviruses, including SARS-CoV-2 (Shi et al., 2020).

The three best characterised members of the IFITM family are IFITM1, IFITM2 and IFITM3 (Bailey et al., 2014; Perreira et al., 2013; Shi et al., 2017; Smith et al., 2014). They contain different sorting motifs and IFITM1 is mainly localised at the plasma membrane, while IFITM2 and 3 are found inside the cell on endo-lysosomal membranes (Bailey et al., 2014). The molecular mechanism(s) underlying the target cell antiviral activity of IFITMs are not fully understood. However, recent reports suggest that they modulate membrane rigidity and curvature to prevent fusion of the viral and cellular membranes (Li et al., 2013; Shi et al., 2017; Zani and Yount, 2018).

Here, we examined whether IFITMs may restrict SARS-CoV-2. In agreement with previous reports on SARS- and MERS-CoV (Huang et al., 2011; Wrensch et al., 2014) and very recent data on SARS-CoV-2 (Shi et al., 2020), we found that overexpression of IFITMs blocks entry mediated by the SARS-CoV-2 S protein, with IFITM1 and IFITM2 being more potent than IFITM3. Contrary to our expectations, however, siRNA-mediated knock-down of IFTIMs strongly reduced the efficiency of SARS-CoV-2 replication in human lung cells. In particular, endogenous IFITM2 expression was critical for efficient entry of genuine SARS-CoV-2. Our results suggest that SARS-CoV-2 hijacks IFITMs for efficient replication and spread under physiological conditions.

RESULTS

IFITMs block SARS-CoV-2 S-mediated pseudoparticle infection

To examine whether IFITM proteins inhibit SARS-CoV-2 S-dependent viral entry, we used HEK293T transiently expressing ACE2 and pseudotyped viral particles. Specifically, Vesicular-Stomatitis-Virus (VSV) containing a *luciferase* reporter gene instead of the open reading frame for its Glycoprotein (VSV(luc)ΔG) was pseudotyped with the SARS-CoV-2 S protein (Figure 1A). HEK293T cells overexpressing the individual IFITMs were exposed to these pseudoparticles (pp) and the levels of infection quantified by luciferase assay. We found that overexpression of IFITM1 and IFITM2 inhibits SARS-CoV-2 S-mediated VSVpp infection dose-dependently by up to two orders of magnitude, while IFITM3 was less effective (Figure 1B). As control, we used PSGL-1 a broad-spectrum inhibitor of virus attachment (Fu et al., 2020) and confirmed that it prevents SARS-CoV-2 S-mediated infection (He et al., 2020). None of the IFITMs prevented VSV-G dependent entry (Figure S1A). Thus, the inhibitory effect was SARS-CoV-2 S-specific. Potent inhibition of SARS-CoV-2 S-mediated infection by IFITMs was confirmed using lentiviral pseudoparticles (Figure 1C).

It has been reported, that IFITMs can be incorporated into budding HIV-1 virions and reduce their infectivity (Tartour et al., 2014). Thus, we also examined whether IFITMs expression in the virus producer cells affects the infectious titer of SARS-CoV-2 S VSVpp (Figure 1D). However, overexpression of IFITMs in the producer cells had little if any restrictive effects (Figure 1E). IFITM1 even slightly increased VSVpp infectivity at low expression levels (Figure 1E), possibly because it moderately enhances incorporation of the SARS-CoV-2 S protein into VSV particles (Figure S1B). Again, IFITM expression in the producer cells had no effect on VSV-G containing particles (Figure S1C).

To examine the effect of endogenous IFITM expression on S-mediated VSVpp infection, we performed siRNA knock-down (KD) studies in the human epithelial lung cancer cell line Calu-3,

126 which expresses ACE2 and all three IFITM proteins (Figure S1D). Silencing of endogenous IFITM
127 expression enhanced infection mediated by the SARS-CoV-2 S protein about 3- to 7-fold and similar
128 results were obtained with VSVpp containing the SARS-CoV S protein (Figure 1F). Altogether, these
129 data show that transient and endogenous IFITM expression inhibit SARS-CoV-2 S-mediated viral
130 entry in single-round pseudoparticle infection assays.

131 **IFITMs impair SARS-CoV-2 S-mediated membrane fusion**

132 IFITM proteins inhibit viral infections by preventing fusion between the viral and cellular membranes
133 (Shi et al., 2017; Zani and Yount, 2018). To determine whether IFITMs also affect cell-to-cell fusion
134 mediated by the SARS-CoV-2 S protein and the ACE2 receptor, we used a split-GFP assay (Figure
135 S2A). All three IFITMs inhibited fusion between SARS-CoV-2 S and ACE2 expressing HEK293T
136 cells in a dose-dependent manner (Figure 2A). To analyse the impact of IFITMs on S-mediated fusion
137 between virions and target cells, we used HIV-1 particles containing β-lactamase-Vpr fusions as
138 previously described (Cavrois et al., 2014), except that the virions contained the SARS-CoV-2 S
139 instead of the HIV-1 Env protein. Expression of IFITM1, 2 or 3 all prevented fusion of SARS-CoV-
140 2 S HIVpp with ACE2 expressing target cells (Figure 2B).

141 To examine whether endogenous IFITM expression affects the interaction between the S protein
142 on VSVpp and the ACE2 receptor on the target cells, we performed proximity ligation assays (PLA)
143 assays in Calu-3 cells. siRNA silencing of IFITM1, 2 and 3 significantly increased the numbers of
144 PLA foci (Figure 2C). Thus, IFITMs reduce the number of S molecules that are in close proximity to
145 the ACE2 receptor after VSVpp exposure. To further investigate this, HeLa cells were depleted of
146 endogenous IFITM1 and 3 (they do not express IFITM2), transfected with an ACE2 expression
147 vector, and exposed to S-containing VSVpp. In agreement with the results obtained in Calu-3 cells,
148 KD of IFITM1 or IFITM3 increased the number of S/ACE2 foci by about 4- and 10-fold, respectively

(Figures S2B, S2C). Taken together, our results show that all three IFITMs prevent SARS-CoV-2 S/ACE2-mediated attachment and membrane fusion in single round pseudotype infection assays.

Susceptibility of S proteins of SARS-CoV-2 and related CoVs to IFITM overexpression

It has been reported that overexpression of IFITMs inhibits the function of the S proteins of the two previously emerging highly pathogenic SARS- and MERS-CoV (Huang et al., 2011; Wrensch et al., 2014) and SARS-Co-2 (Shi et al., 2020). However, whether the two human SARS CoVs differ in their susceptibility to IFITM-mediated inhibition and whether the sensitivity of SARS-CoV-2 changed after zoonotic transmission is not known. To examine this, we analysed the S proteins of the two human viruses (SARS-CoV-2, SARS-CoV) and the bat (RaTG13-CoV) and pangolin viruses (Pang-CoV) that are closely related to SARS-CoV-2 (Figure S2D) (Lam et al., 2020; Zhou et al., 2020). VSVpp harbouring the various S proteins were used to transduce HEK293T cells coexpressing individual IFITMs and ACE2. Pseudoparticles of SARS-CoV-2 and its closest animal relatives RaTG13-CoV and Pang-CoV showed similar patterns and degrees of sensitivity to overexpression of IFITM1, 2 and 3 (Figure 2D). SARS-CoV S pseudovirions were also efficiently restricted by IFITM1 and 2 and even more susceptible to inhibition by IFITM3 than SARS-CoV-2 S pseudovirions. Altogether, our results showed that the susceptibility of SARS-CoV-2 to inhibition by IFITMs did not markedly change after zoonotic transmission at least in transfected HEK293T cells.

Determinants of IFITM-mediated inhibition of SARS-CoV-2 S in HEK293T cells

Previous analyses showed that the antiviral activity of IFIM proteins is modulated by ubiquitination and palmitoylation (Narayana et al., 2015; Yount et al., 2010). To analyse whether these post-transcriptional modifications also impact their ability to prevent SARS-CoV-2 S-mediated infection, we generated ubiquitination and palmitoylation defective mutants of IFITM1, 2 and 3 (Figure S2E). As expected, ubiquitination- and palmitoylation-defective mutants of IFITM2 and IFITM3 showed reduced activity in counteracting SARS-CoV-2 S-mediated entry of VSVpp (Figure S2F). It has been

documented that a Y20A mutation or deletion of the N-terminal 21 amino acids of IFITM3 converts this restriction factor to an enhancer of MERS-CoV or SARS-CoV S-mediated entry (Jia et al., 2012; Zhao et al., 2019). In line with these findings and recent data on SARS-CoV-2 (Shi et al., 2020), both N-terminal mutants of IFITM3 moderately enhanced VSVpp entry via the SARS-CoV-2 S protein (Figure S2F,G) upon transient overexpression or stable expression in HEK293T cells. Thus, specific mutations convert IFITM3 from an inhibitor to an enhancer of SARS-CoV-2 S-mediated VSVpp infection in transfected HEK293T cells.

Overexpression of IFITMs inhibits wildtype SARS-CoV-2 infection in HEK293T cells

To determine whether IFITMs also prevent infection by genuine SARS-CoV-2, we infected HEK293T cells overexpressing ACE2 alone or together with IFITMs with a wildtype isolate of SARS-CoV-2 at an MOI of 0.05 and measured viral RNA yields in the culture supernatants by qPCR two days later. On average, overexpression of IFITM1 and 2 reduced viral RNA yields by 31.7- and 135.5-fold, respectively (Figure 3A, S3). In comparison, IFITM3 had more modest effects but also achieved about 5-fold inhibition at higher dose, while PSGL-1 reduced virus yields by 14.2-fold (Figure 3A). Thus, in agreement with the inhibitory effects observed using SARS-CoV-2 S VSV or HIV pseudoparticles, overexpression of the three IFITM proteins in HEK293T cells strongly inhibited replication of genuine SARS-CoV-2. Similar to the results obtained on S-mediated VSVpp infection (Figure 1B), overexpression of IFITM1 was most and IFITM3 least effective in preventing wildtype SARS-CoV-2 replication in HEK293T cells.

IFITMs are expressed in relevant tissues and induced upon IFN stimulation

To better assess the potential relevance of the different IFITMs in restricting SARS-CoV-2 replication in infected individuals, and Calu-3 cells as a model, we compared expression levels of IFITM proteins in primary human lung bronchial epithelial cells (NHBE), and human intestinal organoids derived from pluripotent stem cells with Calu-3 cells. These cell types and organoids

represent the sites of SARS-CoV-2 entry and subsequent spread, i.e. the lung and the gastrointestinal tract (Hoffmann et al., 2020a; Krüger et al., 2020; Lamers et al., 2020). Western Blot analyses showed that IFITM2 and 3 are constitutively expressed at low levels in Calu-3 cells and NHBE (Figure 3B). Treatment with IFN-α, β or γ generally induced the expression of all three IFITM proteins, albeit with different efficiencies in different cell types. For example, IFN-β was highly effective in inducing IFITM1 and IFITM2 in NHBE, while IFN-γ most efficiently increased IFITM1 expression levels in Calu-3 cells (Figure 3B). Expression of IFITM1 at the plasma membrane was clearly visible in gut organoids using confocal microscopy upon IFN-β stimulation (Figure 3C). Similarly, upon stimulation, IFITM2 and IFITM3 display a cytoplasmic or vesicle-like localization as previously described (Huang et al., 2011). In summary, IFN inducibility and basal expression of IFITM proteins in lung cells and primary tissues relevant for SARS-CoV-2 infection clearly support a role of IFITMs for viral spread *in vivo*. Our finding that Calu-3 cells express similar endogenous and IFN induced levels of IFITMs as primary lung cells support their relevance for studies on SARS-CoV-2 infection.

Endogenous IFITM expression enhances SARS-CoV-2 entry and replication

Thus far, our results strongly suggested that IFITM proteins are efficient inhibitors of SARS-CoV-2 S-mediated viral entry. To verify this under conditions more closely reflecting the *in vivo* situation, we examined the impact of endogenous IFITM expression on genuine SARS-CoV-2 infection of human lung cells. To this end, we treated Calu-3 cells with siRNAs targeting IFITM1, 2 and 3 or a combination thereof (Figure S4A), infected them with SARS-CoV-2, and determined the levels of cell-associated viral RNA early after viral exposure as indicator of viral entry. It came as surprise that silencing of endogenous IFITM expression severely impaired SARS-CoV-2 infection. At 6 h post-infection depletion of IFITMs 1, 2 and 3 reduced the levels of cell-associated viral RNA about 3-, 22- and 4-fold, respectively (Figure 4A). The effects of IFITM1 and 3 silencing were similar at 24 h

post-infection, while reduced expression of IFITM2 even decreased viral entry by more than two orders of magnitude at this later time point (Figure 4B).

Our findings showed that endogenous expression of IFITM proteins in human lung cells does not restrict but strongly promotes SARS-CoV-2 infection. To further examine this, we determined the levels of cell-free SARS-CoV-2 RNA at 24 h post-infection. In agreement with the effects on cell-associated viral loads, silencing of IFITMs 1, 2 and 3 reduced SARS-CoV-2 RNA yield in the culture supernatants on average by 5.2-, 65.7- and 2.9-fold respectively (Figure 4C). Independent experiments, in which supernatants were harvested 48 h post infection, confirmed that endogenous IFITM expression is critical for efficient SARS-CoV-2 replication in Calu-3 cells (Figure 4D).

In the absence of IFN treatment, KD of IFITMs generally reduced SARS-CoV-2 RNA production (Figure 4A-D). In some experiments, IFN-β treatment prevented SARS-CoV-2 replication almost entirely and silencing of IFITMs had only modest additional effects (Figure 4B, 4C). However, the dependency of SARS-CoV-2 on IFITM proteins for effective virus production was confirmed under non-saturating conditions, when IFN-β reduced but not fully prevented SARS-CoV-2 replication. For example, IFN-β treatment reduced SARS-CoV-2 RNA levels on average about 22-fold at 48 h post-infection and KD of IFITM1, 2 and 3 further reduced viral RNA yields by factors of 35.4-, 67.5- and 8.9-fold, respectively (Figure 4D, S4B, C). To determine differences in the infectious titer, we infected Vero cells with supernatants from the IFN-ß treated Calu-3 cells and determined the virus-induced cytopathic effects (CPE). After infection with supernatants obtained from Calu-3 cells treated with the control siRNA analysis CPE was visible up to a dilution of 10^{-6}, indicating the presence of infectious SARS-CoV-2 (Figure S4D). The virus-induced CPE was drastically reduced upon siRNA mediated knockdown of IFITM proteins. Upon depletion of IFITM1 modest CPE was only observed at a dilution of 10^{-2}, while silencing of IFITM3 expression reduced the CPE caused by infectious SARS-CoV-2 down to a dilution of 10^{-3}. No virus-induced CPE was observed at any dilution upon depletion of IFITM2 or all three IFITM proteins (Figure S4D). This result indicates

that lack of IFITM2 expression reduced infectious SARS-CoV-2 yield by more than four orders of magnitude. Our finding that IFITM2 had the strongest effect agrees with the results of the qPCR assays. Notably, titration experiments showed that IFITMs do not promote genuine SARS-CoV-2 infection in HEK239T cells over a broad range of expression levels (Figure S4E). Thus, the opposing effects of IFITMs on SARS-CoV2 infection in HEK293T and Calu-3 cells do apparently not just dependent on different expression levels.

While all three IFITM proteins promoted SARS-CoV-2 replication in Calu-3 cells, IFITM2 had by far the strongest effect. To obtain first insight into a possible role of IFITMs as SARS-CoV-2 entry cofactors, we infected Calu-3 cells with the wildtype virus and performed PLA assays to detect possible interactions between the viral S protein and the three IFITM proteins. In agreement with a potential role as cofactor for SARS-CoV-2 infection, a significant number of IFITM2/S foci were detectable, while only a few signals were observed for IFITM1 and IFITM3 (Figure 4E). Taken together, our data suggest that IFITM2 is an important cofactor of SARS-CoV-2 entry into human lung cells.

DISCUSSION

The present study demonstrates that endogenous expression of IFITMs is required for efficient replication of SARS-CoV-2 in a human lung cell line. This finding came as surprise since IFITMs are well known as important effectors of innate antiviral immunity and have been shown to inhibit SARS-CoV, MERS-CoV and, very recently, SARS-CoV-2 S pseudotype infection in overexpression assays (Huang et al., 2011; Shi et al., 2020; Wrensch et al., 2014). Confirming and expanding these previous studies, we show that overexpression of IFITM proteins in HEK293T cells prevents S-mediated VSVpp and HIVpp fusion as well as genuine SARS-CoV-2 entry. However, exactly the opposite was observed for genuine SARS-CoV-2 upon manipulation of endogenous IFITM expression levels in human lung cells. Silencing of all three IFITM proteins reduced SARS-CoV-2 entry. However, IFITM2 had the most striking effect and our results suggest that silencing of this factor reduced infectious SARS-CoV-2 production by at least four orders of magnitude. Our results provide novel and highly unexpected insights into the role of IFITM proteins in the spread and pathogenesis of SARS-CoV-2 and suggest that these supposedly antiviral factors are hijacked by SARS-CoV-2 as cofactors for efficient entry.

While IFITMs are generally considered to be inhibitors of viral pathogens enhancing effects on infection of human coronaviruses have been reported for specific mutant forms of IFITM3. Specifically, it has been shown that a single point mutation of Y20A converts IFITM3 from an inhibitor to an enhancer of SARS- and MERS-CoV S-mediated pseudoparticle transduction (Zhao et al., 2017). In agreement with recent data (Shi et al., 2020), we confirmed this enhancing effect for VSVpp carrying the SARS-CoV-2 S protein (Figure S2F, S2G). Notably, while IFITMs were reported to inhibit SARS-CoV, 229E, MERS-CoV and SARS-CoV-2 (Huang et al., 2011; Shi et al., 2020; Wrensch et al., 2014), they have been shown to enhance infection of human CoV-OC43, one of the major etiological agents of common cold (Zhao et al., 2014). Unlike SARS-CoV and SARS-CoV-2, CoV-OC43 does not utilize ACE2 as an entry receptor. We found that expression of all three

IFITM proteins enhance SARS-CoV-2 infection of human lung cells, while only IFITM2 and IFITM3 promoted infection by CoV-OC43 in the previous study. Thus, although both human coronaviruses apparently highjack IFITM for efficient infection they show overlapping but distinct preferences for utilization of specific IFITM proteins.

Studies using single-cycle viral pseudoparticles in transfected HEK293T cells have provided important insights into cellular factors restricting viral entry. However, our finding that IFITMs have opposite effects on S-mediated pseudoparticle infection in transiently transfected HEK293T cells and genuine SARS-CoV-2 infection of human lung cells underlines the importance for verification of antiviral effects under more physiological conditions. In addition, the evidence that some other ISGs, such as LY6E and Cholesterol 25-hydrolase (CH25H), impair SARS-CoV-2 replication by blocking the fusion of virions also comes largely from analyses of S pseudotypes and conditions of IFITM overexpression (Pfaender et al., 2020; Zang et al., 2020; Zhao et al., 2020). Thus, the antiviral effect of presumed inhibitory factors of SARS-CoV-2 entry should be challenged under conditions more closely reflecting the *in vivo* situation. For SARS-CoV-2, we have initiated studies in lung and gut organoid systems.

The exact reasons for the opposing effects of overexpressed and endogenous IFITMs exposure to single cycle SARS-CoV-2 S pseudotyped virus and wildtype SARS-CoV-2 remain to be determined. Previous studies suggested that the subcellular localization, membrane curvature, endocytic activity and lipid composition may affect the antiviral activity of IFITM proteins (Chesarino et al., 2014; Guo et al., 2020; Zhao et al., 2017). Alterations in any of these viral features might affect the balance between restricting and enhancing effects on viral entry. We found that IFITM2 is about an order of magnitude most potent in enhancing SARS CoV-2 entry and replication compared to IFITM1 and IFITM3 (Figure 4A-D). PLA assays revealed that IFITM2 is frequently in close proximity to the Spike protein after exposure of lung cell to SARS CoV-2 (Figure 4E). Thus, it is tempting to speculate that the SARS CoV-2 Spike protein may interact with IFITM2 to highjack it for efficient viral entry

and we are currently investigating this. Other data show that IFITM overexpression in HEK29T cells inhibits both S-mediated transduction by VSV and HIV pseudoparticles (Figure 1B, 1C), as well as replication of genuine SARS-CoV-2 (Figure 3A). Thus, the enhancing effect was specifically observed for endogenous expression of IFITMs in human lung cells and wildtype SARS-CoV-2. This explains why enhancing effect were missed in previous studies. Importantly, these are the conditions that most closely approximate replication of SARS-CoV-2 in infected individuals.

In summary, our data show that IFITMs which are well-known as broad-spectrum inhibitors of many viral pathogens may serve as entry cofactors for SARS-CoV-2 infection of human lung cells. IFITMs are efficiently induced during the innate immune response in SARS-CoV-2 infected individuals (Blanco-Melo et al., 2020; Hadjadj et al., 2020). Consequently, the ability to utilize IFITMs as infection cofactor may play a key role in the ability of SARS-CoV-2 to invade the lower respiratory tract under inflammatory conditions, which represents a hallmark of severe COVID-19. Thus, it will be interesting to examine whether antibodies to IFITMs may offer novel therapeutic perspectives for the treatment of COVID-19.

ACKNOWLEDGMENTS

We thank Susanne Engelhart, Kerstin Regensburger, Martha Meyer, Regina Burger, Nicole Schrott, Daniela Krnavek for excellent technical assistance. The ACE2 vector and the SARS-CoV-2 S-HA plasmid were kindly provided by Shinji Makino and Stefan Pöhlmann. We thank Karl-Klaus Conzelmann and Stefan Pöhlmann for providing VSVΔG. This study was supported by DFG grants to F.K., J.Mün., K.M.J.S., D.Sa. (CRC 1279, SPP 1923, KM 5/1-1, SP1600/4-1), C.G. (GO2153/3-1) EU's Horizon 2020 research and innovation program to J.M. (Fight-nCoV, 101003555), as well as the BMBF to F.K., D.Sa. and K.M.J.S. (Restrict SARS-CoV-2, protACT and IMMUNOMOD). C.P.B., C.C., and R.G. are part of and R.G. is funded by a scholarship from the International Graduate School in Molecular Medicine Ulm (IGradU).

AUTHOR CONTRIBUTIONS

C.P.B. performed most experiments. R.N. performed experiments with infectious SARS-CoV-2 assisted by F.Z., M.V. performed PLA assays, R.G established methods. C.M.S. generated most expression constructs. T.W and L.W. provided the lentiviral pseudotypes while D.Sc. performed FACS for the Vpr-BlaM assay; E.B. and J.W. performed the HEK293T GFP split fusion assay. J.K., S.H. and A.K. provided, cultured and stimulated gut organoids. L.K. helped with the microscopy analysis of the organoids. C.S. and C.C. performed the experiment in HEK293T cells stably expressing IFITMs. J. Mül., C.C. and J. Mün provided SARS-CoV-2 virus. C.S. and S.St. performed assays in stable IFITM expressing HEK293T. R.G., K.S. and S.S. provided resources. D.Sa., J. Mün and C.G. provided additional resources and comments for the manuscript. K.M.J.S and F.K. conceived the study, planned experiments and wrote the manuscript. All authors reviewed and approved the manuscript.

DECLARATIONS OF INTERESTS

The authors declare no competing interests.

FIGURE LEGENDS

Figure 1. IFITM1, 2 and 3 prevent SARS-CoV-2 S mediated pseudoparticle infection.

(A) Schematic depiction of the assay to assess VSVpp entry.

(B) Quantification of VSV(luc)ΔG*SARS-CoV-2-S entry by luciferase activity in HEK293T cells transiently expressing the indicated proteins and infected 24 h post-transfection with VSV(luc) ΔG*SARS-CoV-2-S (MOI 0.025) for 16 h. Bars represent means of n=3±SEM. Lower panel: Immunoblot of the corresponding whole cell lysates (WCLs) stained with anti-IFITM1, anti-IFITM2, anti-IFITM3, anti-PSGL-1, anti ACE2 and anti-actin.

(C) Quantification of VSV(luc) ΔG*SARS-CoV-2-S entry by luciferase activity in HEK293T cells transiently transfected with indicated expression vectors and transduced 24 h post-transfection with HIV(luc)Δ*env**-SARS-CoV-2 S for 48 h. All bar diagrams in this figure represent means of n=3 (±SEM).

(D) Schematic depiction of the assay to assess the effects of IFITMs in the producer cells on SARS-CoV-2 S VSVpp production and infectivity.

(E) Quantification of VSV(luc) ΔG*SARS-CoV-2-S particle infectivity by luciferase activity in Caco-2 cells infected with the supernatant of HEK293T cells transiently transfected with SARS-CoV-2 Spike and indicated expression vectors. Bars represent means of n=3±SEM.

(F) Transduction of Calu-3 cells treated with non-targeting (CTRL) or IFITM1, 2 or 3 siRNAs or a combination thereof with VSV(luc) ΔG*SARS-CoV-2-S particles. Transductions efficiencies were determined as described in panel B.

See also Figure S1.

Figure 2. IFITMs prevent SARS-CoV-2 Spike and ACE2 mediated fusion and attachment.

(A) Split-GFP assay measuring cell-cell fusion. GFP1-10 and SARS-CoV-2 Spike expressing HEK293T were co-cultured with GFP11, ACE2 and IFITM expressing HEK293T. Quantification of successful fusion by GFP positive cells (green) normalized to nuclei (left panel). Bars represent means of n=3±SEM. Exemplary fluorescence images (right panel).

(B) Fusion of HIV(Vpr-Blam)Δ*env**-SARS-CoV-2-S with HEK293T cells transiently expressing ACE2 and IFITMs. Quantification of the fusion efficiency by flow cytometry as percentage of (cleaved CCF2)+ cells. Bars represent means of n=2(3 technical replicates each)±SEM. Right panel: Exemplary gating of the raw data.

(C) Proximity Ligation assay between SARS-CoV-2 Spike and ACE2 in Calu-3 depleted of IFITM1, IFITM2 or IFITM3 were infected with pseudotyped S CoV-2 VSV. Lines represent means of n=2 (60-100 cells) ±SEM. DAPI (blue), nuclei. PLA signal (yellow). Scale bar, 20 µm.

(D) Quantification of the entry of VSV(luc)ΔG pseudotyped with indicated spike proteins (SARS-CoV-2, SARS-CoV, RaTG13-CoV, Pang-CoV) by luciferase activity in HEK293T cells transiently expressing indicated proteins and infected 24h post transfection with pseudoparticles (MOI 0.025) for 16 h. Bars represent means of n=3±SEM.

See also Figure S2.

Figure 3. Effect of IFITM overexpression on SARS-CoV-2 infection and IFITM expression levels in primary cells.

(A) Quantification of viral N gene RNA by qRT-PCR in the supernatant of HEK293T 48 h post infection with SARS-CoV-2 (MOI 0.05). Cells transiently express indicated proteins. Lower panel: Immunoblots of whole cell lysates stained with anti-SARS-CoV-2-Spike, anti-IFITM1, anti-IFITM2/3, anti-PSGL-1, anti-ACE2 and anti-actin. Bars represent means of n=3±SEM.

(B) Expression of IFITM1, IFITM2 and IFITM3 after stimulation with IFN-α2 (500 U/ml, 72 h), IFN-β (500 U/ml, 72 h) or IFN-γ (200 U/ml, 72 h) in Calu-3 cells, primary bronchial epithelial cells (NHBE) or stem cell derived gut organoids. Immunoblot of whole cell lysates stained with anti-IFITM1, anti-IFITM2, anti-IFITM3 and anti-actin.

(C) Immunofluorescence images of stem cell derived gut organoids treated as in (B). Cells were stained with anti-IFITM1,2 or 3 (green) or E-Cadherin (green). Nuclei, DAPI (blue). Scale bar, 20 μm.

See also Figure S3.

Figure 4: Endogenous IFITMs promote SARS-CoV-2 replication and entry

(A, B) Quantification of viral N gene RNA by qRT-PCR in Calu-3 cells 6 h post infection with SARS-CoV-2 (MOI 0.05). Values were normalized to GAPDH and calculated relative to the control (set to 100%). Cells were transiently transfected with siRNA either control (CTRL) or targeting IFITM1, 2, 3 (1, 2, 3) as indicated. Additionally, cells were either treated with IFN-β or left untreated. Bars represent means of n=2±SEM.

(C, D) Quantification of viral N gene RNA by qRT-PCR in the supernatant of Calu-3 48 h post infection with SARS-CoV-2 (MOI 0.05). Cells were transiently transfected with siRNA either control (si.NT) or targeting IFITM1, 2 and 3 as indicated. Additionally, cells were either treated with IFN-β or left untreated. Bars represent means of n=4±SEM.

(E) Proximity ligation assay between SARS-CoV-2 S and IFITM1, IFITM2 or IFITM3 in Calu-3 cells infected with SARS-CoV-2 for 2 h at 4°C. Line represent means of n=(60-100 cells)±SEM. DAPI(Blue), nuclei. PLA signal (yellow). Scale bar, 20 μm.

See also Figure S4.

420 **STAR METHODS**

421

422 **KEY RESOURCES TABLE**

REAGENT or RESOURCE	SOURCE	IDENTIFIER
Antibodies		
IRDye 680RD Goat anti-Rabbit IgG (H + L) (1 to 20000)	LI-COR	Cat# 926-68071
IRDye 800CW Goat anti-Mouse IgG (H + L) (1 to 20000)	LI-COR	Cat# 926-32210
IRDye 800RD Goat anti-Rat IgG (H + L) (1 to 20000)	LI-COR	Cat# 925-32219
Rabbit polyclonal anti-IFITM1	Abcam	Cat# ab233545
Rabbit polyclonal anti-IFITM2	Abcam	Cat#ab236735
Rabbit polyclonal anti-IFITM3	Cell signalling	Cat#59212
Rabbit polyclonal anti-ACE2	Abcam	Cat# sc-166755
Rabbit polyclonal anti-PSGL-1	Abcam	Cat#134243
Mouse monoclonal anti VSV-M	Absoulte Antibody	Cat# Ab01404-2.0
SARS-CoV-2 (COVID-19) spike antibody [1A9]	Biozol	Cat#GTX-GTX632604
Rabbit polyclonal anti-beta Actin (1 to 1000)	abcam	Cat# ab8227
Bacterial and Virus strains		
VSVΔG(luc)*VSV-G	Gert Zimmer (Rentsch and Zimmer, 2011)	N/A
VSVΔG(GFP)*VSV-G	Karl-Klaus Conzelmann,	N/A
BetaCoV/Netherlands/01/NL/2020	European Virus Archive	#010V-03903
BetaCoV/ France/IDF0372/2020	European Virus Archive	#014V-03890
Chemicals, Peptides, and Recombinant Proteins		
L-Glutamine	Pan Biotech	Cat# P04-80100
Dulbecco's Modified Eagle Medium (DMEM)	Gibco	Cat#41965039
Minimum Essential Medium Eagle (MEM)	Sigma-Aldrich	Cat#M4655
Opti-MEM	Gibco	Cat# M3942
Roswell Park Memorial Institute (RPMI)	Gibco	Cat# 22400089
Penicillin-Streptomycin	ThermoFisher	Cat# 15140122
non-essential amino acids	Sigma-Aldrich	Cat# M7145
Sodium pyruvate	Sigma-Aldrich	Cat# S8636
FCS	Gibco	Cat#10270106
Trypsin EDTA	Gibco	Cat# T3924
TMB peroxidase substrate (Sure blue)	Medac	Cat# 52-00-04
Crystal violet	Sigma-Aldrich	Cat# C0775
Avicel	FMC Corporation	Cat# RC-581

hESC Matrigel	Corning	Cat#354277
TrypLE Express	Invitrogen	Cat#12605036
Antibody diluent	Zytomed	Cat#ZUC025-100
Fluoromount-G	Southern Biotech	Cat#0100-01
NucRed Live 647 ReadyProbes Reagent	Invitrogen	Cat#R37106
Solution D	ThermoFisher	Cat# K1156
Loading kit with CCF2-AM	ThermoFisher	Cat#K1032
Lipofectamine RNAiMAX	ThermoFisher	Cat# 13778075
Luciferase Assay Kit	Promega	Cat# E1500
Hoechst 33342	Invitrogen	Cat#62249
Q5 Site-Directed Mutagenesis Kit	NEB	Cat# E0554
TaqMan Fast Virus 1-Step Master Mix	ThermoFisher	Cat# 4444436
Duolink In Situ Detection Reagents FarRed	Sigma-Aldrich	Cat#DOU92013
GAPD (GAPDH) Endogenous Control	ThermoFisher	Cat#4352338E
β-mercaptoethanol	Sigma-Aldrich	Cat# 444203
Immobilon-FL PVDF membranes	Merck Millipore	Cat#IPVH00010
Paraformaldehyde	Merck, Darmstadt	Cat# 104005
TransIT-LT1	Mirus	Cat#MIR2300
NuPAGE 4±12% Bis-Tris Gels	ThermoFisher	Cat# NP0321BOX
Synthetic SARS-CoV-2-RNA	Twist Bioscience	Cat# 102019
RNAiMAX	ThermoFisher	Cat# LMRNA015
Recombinant IFN-α2	pbl assay science	Cat# 11101-1
Recombinant IFN-β	R&D systems	Cat# 8499-IF-010
Recombinant IFN-γ	Sigma-Aldrich	Cat# I3265
Agarose	Sigma-Aldrich	Cat#A9539
Poly-L-Lysine Solution	Merck, Darmstadt	Cat# A005C
Experimental Models: Cell Lines		
Human: Calu-3	Manfred Frick	N/A
Human: Caco-2	Holger Barth	N/A
Human: HeLa	ATCC	Cat# CRM-CCL-2
Hybridoma cells	ATCC	CRL-2700
Human: HEK293T GFP1-10 and GFP11 split	Olivier Schwarz	N/A
African Green Monkey: Vero E6	ATCC	Cat# CRL-1586
Human: Normal Human Bronchial Epithelial cells (NHBE)	Lonza	Cat# CC-2540
Human: Embryonic Stem Cell (hESC) line HUES8	Harvard University	N/A
Oligonucleotides		
XbaI_forward: CGTCTAGAGCCACCATG	This paper	N/A
XbaI_nCoV-2_S_Forward: CGTCTAGAATGTTTCTGCTGACCACCAAGC GGACCATG	This paper	N/A
nCoV-2_S_V5_ MluI_reverse: GCACGCGTCTACGTAGAATCGAGACCGAGG AGAGGGTTAGGGATAGGCTTACCACCAGAA CCGGTGTAGTGCAGTTTCACGCCCTTC	This paper	N/A

Pangolin-S_MluI_reverse: GCACGCGTCTCAATTTTCCGTTTGAGGGTAAAACACAGAG	This paper	N/A
RaTG13-S_MluI_reverse: CGACGCGTCTAGGTGTAGTGCAGCTTCACG	This paper	N/A
IFI1_K122A_forward: AATACAGGAAGCCCGGGGTTACTACCCATACG	This paper	N/A
IFI1_K122A_reverse: ATCTGTAACATAATATGGTAGACTG	This paper	N/A
CTRL siRNA-01: UAAGGCUAUGAAGAGAUAC	This paper	D-001206-14-20
CTRL siRNA-02: AUGUAUUGGCCUGUAUUAG	This paper	D-001206-14-21
CTRL siRNA-03: AUGAACGUGAAUUGCUCAA	This paper	D-001206-14-22
CTRL siRNA-04: UGGUUUACAUGUCGACUAA	This paper	D-001206-14-23
siRNA IFITM2-01: CAAACCUUCUCUCCUGUCA	Dharmacon	D-020103-01
siRNA IFITM2-02: UCAAGGAGGAGCAGGAAGU	Dharmacon	D-020103-02
siRNA IFITM2-03: UCGUCCAGGCCCAGCGAUA	Dharmacon	D-020103-03
siRNA IFITM2-04: UGGUCUGGUCCCUGUUCAA	Dharmacon	D-020103-18
siRNA IFITM3-01: ACGUGUUUCUGGUGCUAAA	Dharmacon	D-014116-13
siRNA IFITM3-02: AUGGAUAGAUCAGGAGGCA	Dharmacon	D-014116-14
siRNA IFITM3-03: UGCUGAUCUUCCAGGCCUA	Dharmacon	D-014116-15
siRNA IFITM3-04: UCGUCAUCCCAGUGCUGAU	Dharmacon	D-014116-16
HKU-NF forward: TAATCAGACAAGGAACTGATTA	Biomers	N/A
HKU-N reverse: CGAAGGTGTGACTTCCAT G	Biomers	N/A
HKU-N Probe: FAM-GCAAATTGTGCAATTTGCGG-TAMRA	Biomers	N/A
Recombinant DNA		
pCG_IFITM1	This paper	N/A
pCG_IFITM2	This paper	N/A
pCG_IFITM3	This paper	N/A
pCG_IFITM1-IRES_eGFP	This paper	N/A
pCG_IFITM2-IRES_eGFP	This paper	N/A
pCG_IFITM3-IRES_BFP	This paper	N/A
pQCXIP IFITM1	Stephen Elledge	N/A

pQCXIP IFITM2	Stephen Elledge (Huang et al., 2011)	N/A
pQCXIP IFITM3	Stephen Elledge	N/A
pQCXIP IFITM1-HA	This paper	N/A
pQCXIP IFITM2-HA	This paper	N/A
pQCXIP IFITM3-HA	This paper	N/A
pQCXIP IFITM1 Δ palm (C 50, 51, 84 A)-HA	This paper	N/A
pQCXIP IFITM2 Δ palm (C 70, 72, 104 A)-HA	This paper	N/A
pQCXIP IFITM3 Δ palm (C 71, 72, 105 A)-HA	This paper	N/A
pQCXIP IFITM1 Δ ubi (K 3, 62, 67, 83A)-HA	This paper	N/A
pQCXIP IFITM2 Δ ubi (K 23, 82, 87, 103 A)-HA	This paper	N/A
pQCXIP IFITM3 Δ ubi (K 24, 83, 88, 104 A)-HA	This paper	N/A
pQCXIP IFITM1 Δ ubi (K 3, 62, 67, 83, 122 A)-HA	This paper	N/A
pCG_SARS-CoV2-Spike-IRES_eGFP	Stefan Pöhlmann(Hoffmann et al., 2020a)	N/A
pCG_SARS-CoV2-Spike C-V5-IRES_eGFP	This paper	N/A
pCG_Pangolin CoV- spike (humanized)	This paper	N/A
pCG_batCoV-RaTG13-spike-IRES_eGFP(humanized)	This paper	N/A
pCG_SARS-CoV-1-S-IRES_eGFP(humanized)	Michael Schindler	N/A
pLV-EF1a-human ACE2-IRES-puro	This paper	N/A
pCMV4-BlaM-Vpr	Addgene	Cat# 21950
pTargeT-hACE2	Shuetsu Fukushi and Masayuki Saijo (Fukushi et al., 2005)	Cat#16033974
pLV-EF1a-IRES-Puro	Addgene	Cat# 85132
pCX4bsrACE2	Shinji Makino (Kamitani et al., 2006)	N/A
Software and Algorithms		
Corel DRAW 2017	Corel Corporation	https://www.coreldraw.com/
GraphPad Prism Version 8	GraphPad Software, Inc.	https://www.graphpad.com
LI-COR Image Studio Lite Version 5.0	LI-COR	www.licor.com/
Fiji (Image J) version 1.8	Java	www.imagej.nih.gov/ij

423

424

CONTACT FOR REAGENT AND RESOURCE SHARING

Lead contact

Further information and requests for resources and reagents should be directed to and will be fulfilled by the Lead Contacts, Konstantin Sparrer (konstantin.sparrer@uni-ulm.de) and Frank Kirchhoff (frank.kirchhoff@uni-ulm.de).

Materials Availability

All unique reagents generated in this study are listed in the Key Resources Table and available from the Lead Contacts.

EXPERIMENTAL MODEL AND SUBJECT DETAILS

Cell lines. All cells were cultured at 37°C in a 5% CO2 atmosphere. HEK293T and HeLa cells were maintained in Dulbecco's Modified Eagle Medium (DMEM) supplemented with 10% heat-inactivated fetal calf serum (FCS), L-glutamine (2 mM), streptomycin (100 µg/ml) and penicillin (100 U/ml). HEK293T and HeLa cells were provided and authenticated by the ATCC. Caco-2 (human epithelial colorectal adenocarcinoma) cells were maintained in DMEM containing 10% FCS, glutamine (2 mM), streptomycin (100 µg/ml) and penicillin (100 U/ml) and NEAA supplement (Non-essential amino acids (10%)), sodium Pyruvate (10%). Calu-3 (human epithelial lung adenocarcinoma) cells were cultured in Minimum Essential Medium Eagle (MEM) supplemented with 10% FCS (during viral infection) or 20% (during all other times), penicillin (100 µg/ml), streptomycin (100 µg/ml), 1 mM sodium pyruvate, and NEAA supplement (Non-essential amino acids (10%). Hybridoma cells were cultured in Roswell Park Memorial Institute (RPMI) 1640 medium supplemented with 10% fetal calf serum (FCS), L-glutamine (2 mM), streptomycin (100 µg/ml) and penicillin (100 U/ml). Monoclonal anti-VSV-G containing supernatant was aliquoted and stored at -20°C.

Primary cell cultures. Human embryonic stem cell (hESC) line HUES8 (Harvard University) was used with permission from the Robert Koch Institute according to the "79. Genehmigung nach dem Stammzellgesetz, AZ 3.04.02/0084". Cells were cultured on hESC Matrigel (Corning) in mTeSR1 medium (Stemcell Technologies) at 5% CO2, 5% O2, and 37°C. Medium was changed every day and cells were splitted twice a week with TrypLE Express (Invitrogen). Experiments involving human stem cells were approved by the Robert-Koch-Institute (156. Genehmigung nach dem Stammzellgesetz Erteilt) on 29.04.2020. NHBE (primary human bronchial/tracheal epithelial) cells were grown in Bronchial Epithelial Cell Growth Basal Medium (BEGM) and Bronchial Epithelial Cell Growth Medium SingleQuots Supplements and Growth Factors.

METHOD DETAILS

Expression constructs. pQCXIP with HA-tagged IFITM proteins was generated by adding an HA-tag to pQCXIP-IFITM1/2/3. Expression plasmids encoding for IFITM1, IFITM2 and IFITM3 (pCG_IFITM1, pCG_IFITM2, pCG_IFITM3 and pCG_IFITM1-IRES_eGFP, pCG_IFITM2-IRES_eGFP and pCG_IFITM3-IRES_BFP) were PCR amplified and subcloned in pCG and pCG-IRES-eGFP-backbones using flanking restriction sites XbaI and MluI from pQCXIP IFITM1-HA, pQCXIP IFITM2-HA, pQCXIP IFITM3-HA, that with pQCXIP IFITM1Δpalm (C 50, 51, 84 A)-HA, pQCXIP IFITM2Δpalm (C 70, 72, 104 A)-HA , pQCXIP IFITM3Δpalm (C 71, 72, 105 A)-HA , pQCXIP IFITM1Δubi (K 3, 62, 67, 83A)-HA , pQCXIP IFITM2Δubi (K 23, 82, 87, 103 A)-HA and pQCXIP IFITM3Δubi (K 24, 83, 88, 104 A)-HA. The pQCXIP IFITM mutant plasmids were generated using Q5 Site-Directed Mutagenesis Kit (NEB). pCG_SARS-CoV-2-Spike-IRES_eGFP (humanized), encoding the spike protein of SARS-CoV-2 isolate Wuhan-Hu-1, NCBI reference Sequence YP_009724390.1, was kindly provided by Stefan Pöhlmann (German Primate Center, Göttingen, Germany) while pCG_SARS-CoV2-Spike C-V5-IRES_eGFP was PCR amplified and

475 subcloned using XbaI+MluI. Constructs coding SARS-CoV-S, Pangolin CoV-S were ordered at
476 TwistBioscience or RaTG13-S at Baseclear and subcloned using XbaI+MluI into pCG-IRES_eGFP
477 backbone. To generate the pLV-EF1a-human ACE2-IRES-puro, pTargeT-hACE2 was provided by
478 Shuts Fukushi and Masayuki Saijo (National Institute of Infectious Diseases, Tokyo, Japan). The
479 plasmid of human ACE2 was digested with MluI and SmaI and then the DNA fragment was inserted
480 into the MluI-HpaI site of pLV-EF1a-IRES-Puro.
481
482 **Pseudoparticle stock production**. To produce pseudotyped VSV(luc/GFP)ΔG particles, HEK293T
483 cells were transfected with pCG_SARS-CoV-2-Spike C-V5-IRES_GFP, pCG_SARS-CoV-Spike C-
484 V5-IRES_GFP, pCG_Pangolin CoV-spike (humanized) or pCG_batCoV-RaTG13-spike-
485 IRES_eGFP (humanized) using PEI (1 mg/mL) or pCG_SARS-CoV-1 S-IRES_eGFP (humanized)
486 as previously described (Koepke et al., 2020). 24 hours post transfection, the cells were infected with
487 VSVΔG(GFP/luc)*VSV-G at an MOI of 1. One hour post infection, the inoculum was removed.
488 Pseudotyped particles were harvested twice at 16 h post infection. Cell debris were pelleted by
489 centrifugation at at 2000 rpm for 5 min. Residual input particles carrying VSV-G were blocked by
490 adding 10 % (v/v) of I1 Hybridoma Supernatant (I1, mouse hybridoma supernatant from CRL-2700;
491 ATCC) to the cell culture supernatant.
492 To produce pseudotyped HIV-1(fLuc)Δenv particles, HEK293T cells were transfected with
493 pCMVdR8.91 and pSEW-luc2 or pCMV4-BlaM-vpr as well as pCG_SARS-CoV-2-Spike C-V5-
494 IRES_eGFP using TransIT-LT1 according to the manufacturers protocol. Six hours post transfection,
495 the medium was replaced with DMEM containing only 2.5% FCS. The particles were harvested
496 48 hours post transfection. Cell debris were pelleted and removed by centrifugation at at 2000 rpm
497 for 5 min.
498

Target cell assay. HEK293T cells were transiently transfected using PEI (Koepke et al., 2020) with pLV-EF1a-human ACE2-IRES-puro and pCG-IFITM1-IRES_eGFP or pCG-IFITM2-IRES_eGFP or pCG-IFITM3-IRES_BFP. 24h post transfection the cells were transduced/infected with HIV-1Δenv(fLuc)* SARS-CoV-2 S or VSV(luc)ΔG*SARS-CoV-2 S particles. 16h post infection the cells were lysed in 300µl of Luciferase Lysis buffer (Promega) and firefly luciferase activity was determined using the Luciferase Assay Kit (Promega) according to the manufacturer's instructions on an Orion microplate luminometer (Berthold).

Producer cell assay. HEK293T cells were transiently transfected using PEI (Koepke et al., 2020) with pCG_IFITM1 IRES_eGFP, pCG_IFITM2-IRES_eGFP, pCG_IFITM3-IRES_BFP or pCG_SARS-CoV-2-Spike-C-V5-IRES_eGFP. 24 h post transfection cells were infected with VSV(GFP)ΔG*SARS-CoV-2 S or VSV(GFP)ΔG*VSV-G with a MOI of 1. After 1 hour, the inoculum was removed and medium was replaced. 16h post infection, cells were harvested to generate cell lysates. The supernatant was collected separately and supplemented with 10 % (v/v) of I1 Hybridoma Supernatant. Blocked supernatants were used to infect Caco-2 cells. 16h post infection medium was removed and cells were washed with PBS, detached with Trypsin-EDTA (Gibco) and fixed with 2% PFA for 30 min at 4°C. GFP-positive cells were analysed by flow cytometry (BD Canto II and FlowJo).

Luciferase assay. To determine viral gene expression, the supernatant of transfected cells was removed 16 h and 48 h post infection and the cells lysed in 300µl of Luciferase Lysis buffer (Luciferase Cell Culture Lysis, Promega). 16h post infection, and firefly luciferase activity was determined using the Luciferase Assay Kit (Luciferase Cell Culture, Promega) according to the manufacturer's instructions on an Orion microplate luminometer (Berthold).

Vpr-BlaM fusion assay. HEK293T cells were seeded and transiently transfected using PEI (Koepke et al., 2020) with pLV-EF1a-human_ACE2-IRES-puro and pCG_IFITM1, pCG_IFITM2 or pCG_IFITM3. 24 hours post transfection, cells were transferred to a 96-well plate. On the next day, cells were infected with 50µl HIV-1 Δenv (BlaM-Vpr)-*SARS-CoV-2-S particles for 2.5 h at 37 °C, followed by washing with PBS. Cells were detached and stained with CCF2/AM (1 mM) as previously described(Cavrois et al., 2002). Finally, cells were washed and fixed with 4% PFA. The change in emission fluorescence of CCF2 after cleavage by the BlaM-Vpr chimera was monitored by flow cytometry using a FACSCanto II (BD).

IFITM expressing HEK293T cells assay. HEK293T cells were stably transduced with ACE2 (pCX4bsrACE2) and indicated IFITM-HA (pQCXIP) constructs. Upon selection with blasticidin and puromycin and confirmation of ACE2 and IFITM-HA expression by flow cytometry, cells were transduced with lentiviral particles pseudotyped with C-terminally HA-tagged SARS-CoV-2 spike and expressing luciferase. Luminometric measurement occurred 48 hours post transduction.

SARS-CoV-2 virus stock production. BetaCoV/Netherlands/01/NL/2020 or BetaCoV/ France/IDF0372/2020 was propagated on Vero E6 infected at an MOI of 0.003 in serum-free medium containing 1 µg/ml trypsin as previously described (Nchioua et al., 2020). Briefly, the cells were inoculated for 2 h at 37°C before the inoculum was removed. The supernatant was harvested 48 h post infection upon visible cytopathic effect (CPE). To remove the debris, the supernatants were centrifuged for 5 min at 1,000 × g, then aliquoted and stored at −80°C. Infectious virus titre was determined as plaque forming units (PFU). N gene RNA copies were determined by RT-qPCR.

Plaque-forming Unit Assay. The plaque-forming unit (PFU) assay was performed as previously described (Nchioua et al., 2020). SARS-CoV-2 stocks were serially diluted and confluent monolayers of Vero E6 cells infected. After incubation for 1 to 3 h at 37°C with shaking every 15 to 30 min. The cells were overlaid with 1.5 ml of 0.8 % Avicel RC-581 (FMC) in medium and incubated for 3 days. Cells were fixed with 4 % paraformaldehyde (PFA) at room temperature for 45 min. After the cells were washed with PBS once 0.5 ml of staining solution (0.5 % crystal violet and 0.1 % triton in water). After 20 min incubation at room temperature, the staining solution was removed using water, virus-induced plaque formation quantified, and PFU per ml calculated.

qRT-PCR. N (nucleoprotein) RNA levels were determined in supernatants or cells collected from SARS-CoV-2 infected HEK293T or Calu-3 cells 6 h, 24 h or 48 h post-infection. Total RNA was isolated using the Viral RNA Mini Kit (Qiagen) according to the manufacturer's instructions. RT-qPCR was performed according to the manufacturer's instructions using TaqMan Fast Virus 1-Step Master Mix (Thermo Fisher) and a OneStepPlus Real-Time PCR System (96-well format, fast mode). Primers were purchased from Biomers and dissolved in RNAse free water. Synthetic SARS-CoV-2-RNA (Twist Bioscience) were used as a quantitative standard to obtain viral copy numbers. All reactions were run in duplicates. (Forward primer (HKU-NF): 5'-TAA TCA GAC AAG GAA CTG ATT A-3'; Reverse primer (HKU-NR): 5'-CGA AGG TGT GAC TTC CAT G-3'; Probe (HKU-NP): 5'-FAM-GCA AAT TGT GCA ATT TGC GG-TAMRA). GAPDH primer/probe sets (Thermo Fisher) were used for normalization of cellular RNA levels.

IFITM1, 2 and 3 knockdown. 24 h and 96 h post-seeding cells were transfected with 20 µM twice (Calu-3) or once 24 h post seeding with 40 µM (HeLa cells) of either non-targeting siRNA or IFITM1, IFITM2 or IFITM3 specific siRNA were transfected using Lipofectamine RNAiMAX (Thermo

Fisher) according to the manufacturer's instructions. Prior to transfection, the medium was changed. 14 h post transfection, the medium was replaced with 1 ml MEM supplemented with 500 U/ml IFN-β 7 h post transfection, the Calu-3 cells were infected with SARS-CoV-2 (MOI 0.05) and 7 to 9 h later, supernatant was removed, and 1 ml fresh medium was added. 48h post infection cells and supernatants were harvested for Western blot and qPCR analysis respectively.

Calu-3, NHBE or gut organoid stimulation. Calu-3 and NHBE cells were seeded in 12 well plates. HUES88 were seeded in 24-well-plates were coated with growth factor reduced (GFR) Matrigel (Corning) and in mTeSR1 with 10 µM Y-27632 (Stemcell technologies). The next day, differentiation to organoids was started at 80-90% confluency as previously described (Krüger et al., 2020). Cells or organoids were stimulated with IFN-α2 (500 U/ml), IFN-β (500 U/ml), IFN-γ (200 U/ml). 3 days post stimulation whole cell lysates were generated.

Immunofluorescence of gut organoids. For histological examination, organoids were fixed in 4 % PFA over night at 4°C, washed with PBS, and pre-embedded in 2 % agarose (Sigma) in PBS. After serial dehydration, intestinal organoids were embedded in paraffin, sectioned at 4 µm, deparaffinized, rehydrated and subjected to heat mediated antigen retrieval in tris Buffer (pH 9) or citrate buffer (pH 6). Sections were permeabilized with 0.5 % Triton-X for 30 min at RT and stained over night with primary antibodies (rabbit anti-IFITM1 1:500 or rabbit anti-IFITM2 1:500 or rabbit anti-IFITM3 1:250) diluted in antibody diluent (Zytomed) in a wet chamber at 4°C. After washing with PBS-T, slides were incubated with secondary antibodies (Alexa Fluor IgG H+L, Invitrogen, 1:500) and 500 ng/ml DAPI in Antibody Diluent for 90 min in a wet chamber at RT. After washing with PBS-T and water, slides were mounted with Fluoromount-G (Southern Biotech). Negative controls were performed using IgG controls or irrelevant polyclonal serum for polyclonal antibodies, respectively. Images were acquired using a LSM 710 system.

GFP Split fusion assay. GFP1-10 and GFP11-expressing HEK293T cells were seeded separately at a density of 80.000 cells per well of a 24-well plate. One day post seeding, cells were transiently transfected using the calcium-phosphate precipitation method (Chen and Okayama, 1987). GFP1-10 cells were co-transfected with increasing amounts (0, 8, 16, 32, 64, 125, 250, 500 ng) of pCG_IFTM1, pCG_IFITM2, pCG_IFITM3 and 250 ng of pLV-EF1a-human ACE2-IRES-puro. GFP11 cells were transfected with 250 ng of pCG_SARS-CoV-2-Spike C-V5 codon optimised. 16 h post transfection, GFP1-10 and GFP11 cells were co-cultured in poly-L-lysine-coated 24-well plate. 24 h post co-culturing, cells were fixed with 4 % PFA and cell nuclei were stained using NucRed Live 647 ReadyProbes Reagent (Invitrogen) according to the manufacturer's instructions. Fluorescence imaging of GFP and NucRed was performed using a Cytation3 imaging reader (BioTek Instruments). 12 images per well were recorded automatically using the NucRed signal for autofocusing. The GFP area was quantified using a macro for ImageJ.

Whole cell lysates. To determine expression of cellular and viral proteins, cells were washed in PBS and subsequently lysed in Western blot lysis buffer (150 mM NaCl, 50 mM HEPES, 5 mM EDTA, 0.1% NP40, 500 µM Na_3VO_4, 500 µM NaF, pH 7.5) supplemented with protease inhibitor (1:500, Roche) as previously described (Koepke et al., 2020). After 5 min of incubation on ice, the samples were centrifuged (4°C, 20 min, 14.000 rpm) to remove cell debris. The supernatant was transferred to a fresh tube, the protein concentration was measured and adjusted using Western blot lysis buffer.

SDS-PAGE and Immunoblotting. Western blotting was performed as previously described (Koepke et al., 2020). In brief, whole cell lysates were mixed with 4x or 6x Protein Sample Loading Buffer (LI-COR, at a final dilution of 1x) supplemented with 10 % β-mercaptoethanol (Sigma Aldrich), heated at 95°C for 5 min, separated on NuPAGE 4±12% Bis-Tris Gels (Invitrogen) for 90

minutes at 100 V and blotted onto Immobilon-FL PVDF membranes (Merck Millipore). The transfer was performed a constant voltage of 30 V for 30 minutes. After the transfer, the membrane was blocked in 1 % Casein in PBS (Thermo Scientific). Proteins were stained using primary antibodies against IFITM1 (1:1000,), IFITM2 (1:1000), IFITM3 (1:1000) SARS Spike CoV-2 (1:1000), VSV-M (1:1000), β-actin (1:5000 Abcam,), ACE2 (1:1000) and Infrared Dye labelled secondary antibodies (LI-COR IRDye). Band intensities were quantified using Image Studio (LI-COR).

Proximity Ligation Assay. The proximity ligation assay (PLA) was performed as previously described (Volcic et al., 2020). In brief, HeLa or Calu-3 were seeded in a 24-well plate on a cover slip glass. 24 h post seeding the cells have been transfected once with 40 μM either non-targeting siRNA or IFITM1 or IFITM3 siRNAs or and Calu-3 2 times with 20 μM. 24h post transfection the cells were prechilled for 30 minutes at 4°C and then infected with VSV(luc)ΔG*-SARS-CoV-2 S (MOI 2) or BetaCoV/ France/IDF0372/2020 (MOI 0.05) for 2 h on ice. The cells have been washed once with cold PBS and fixed with 4% PFA. Images were acquired on a Zeiss LSM 710 and processed using ImageJ (Fiji).

QUANTIFICATION AND STATISTICAL ANALYSIS

Statistical analyses were performed using GraphPad PRISM 8 (GraphPad Software). P-values were determined using a two-tailed Student's t test with Welch's correction. Unless otherwise stated, data are shown as the mean of at least three independent experiments ± SEM. Significant differences are indicated as: *, $p < 0.05$; **, $p < 0.01$; ***, $p < 0.001$. Statistical parameters are specified in the figure legends.

REFERENCES

Bailey, C.C., Zhong, G., Huang, I.-C., and Farzan, M. (2014). IFITM-Family Proteins: The Cell's First Line of Antiviral Defense. Annu. Rev. Virol. *1*, 261–283.

Bermingham, A., Chand, M.A., Brown, C.S., Aarons, E., Tong, C., Langrish, C., Hoschler, K., Brown, K., Galiano, M., Myers, R., et al. (2012). Severe respiratory illness caused by a novel coronavirus, in a patient transferred to the United Kingdom from the Middle East, September 2012. Eurosurveillance *17*.

Blanco-Melo, D., Nilsson-Payant, B.E., Liu, W.-C., Uhl, S., Hoagland, D., Møller, R., Jordan, T.X., Oishi, K., Panis, M., Sachs, D., et al. (2020). Imbalanced host response to SARS-CoV-2 drives development of COVID-19. Cell.

Cavrois, M., De Noronha, C., and Greene, W.C. (2002). A sensitive and specific enzyme-based assay detecting HIV-1 virion fusion in primary T lymphocytes. Nat. Biotechnol.

Chen, C., and Okayama, H. (1987). High-efficiency transformation of mammalian cells by plasmid DNA. Mol. Cell. Biol. *7*, 2745–2752.

Chesarino, N.M., McMichael, T.M., and Yount, J.S. (2014). Regulation of the trafficking and antiviral activity of IFITM3 by post-translational modifications. Future Microbiol. *9*, 1151–1163.

Diamond, M.S., and Farzan, M. (2013). The broad-spectrum antiviral functions of IFIT and IFITM proteins. Nat. Rev. Immunol. *13*, 46–57.

Fu, Y., He, S., Waheed, A.A., Dabbagh, D., Zhou, Z., Trinité, B., Wang, Z., Yu, J., Wang, D., Li, F., et al. (2020). PSGL-1 restricts HIV-1 infectivity by blocking virus particle attachment to target cells. Proc. Natl. Acad. Sci. U. S. A. *117*, 9537–9545.

Fukushi, S., Mizutani, T., Saijo, M., Matsuyama, S., Miyajima, N., Taguchi, F., Itamura, S., Kurane,

667 I., and Morikawa, S. (2005). Vesicular stomatitis virus pseudotyped with severe acute respiratory
668 syndrome coronavirus spike protein. J. Gen. Virol.

669 Guo, X., Steinkühler, J., Marin, M., Li, X., Lu, W., Dimova, R., and Melikyan, G.B. (2020).
670 Interferon-Induced Transmembrane Protein 3 Blocks Fusion of Diverse Enveloped Viruses by
671 Locally Altering Mechanical Properties of Cell Membranes. BioRxiv 2020.06.25.171280.

672 Hadjadj, J., Yatim, N., Barnabei, L., Corneau, A., Boussier, J., Smith, N., Péré, H., Charbit, B.,
673 Bondet, V., Chenevier-Gobeaux, C., et al. (2020). Impaired type I interferon activity and
674 inflammatory responses in severe COVID-19 patients. Science.

675 He, S., Hetrick, B., Dabbagh, D., Akhrymuk, I. V., Kehn-Hall, K., Freed, E.O., and Wu, Y. (2020).
676 PSGL-1 blocks SARS-CoV-2 S protein-mediated virus attachment and infection of target cells. (Cold
677 Spring Harbor Laboratory).

678 Hoffmann, M., Kleine-Weber, H., Schroeder, S., Krüger, N., Herrler, T., Erichsen, S., Schiergens,
679 T.S., Herrler, G., Wu, N.-H., Nitsche, A., et al. (2020a). SARS-CoV-2 Cell Entry Depends on ACE2
680 and TMPRSS2 and Is Blocked by a Clinically Proven Protease Inhibitor. Cell.

681 Hoffmann, M., Kleine-Weber, H., and Pöhlmann, S. (2020b). A Multibasic Cleavage Site in the Spike
682 Protein of SARS-CoV-2 Is Essential for Infection of Human Lung Cells. Mol. Cell *78*, 779-784.e5.

683 Huang, I.C., Bailey, C.C., Weyer, J.L., Radoshitzky, S.R., Becker, M.M., Chiang, J.J., Brass, A.L.,
684 Ahmed, A.A., Chi, X., Dong, L., et al. (2011). Distinct patterns of IFITM-mediated restriction of
685 filoviruses, SARS coronavirus, and influenza A virus. PLoS Pathog. *7*.

686 Jia, R., Pan, Q., Ding, S., Rong, L., Liu, S.-L., Geng, Y., Qiao, W., and Liang, C. (2012). The N-
687 Terminal Region of IFITM3 Modulates Its Antiviral Activity by Regulating IFITM3 Cellular
688 Localization. J. Virol. *86*, 13697–13707.

689 Kamitani, W., Narayanan, K., Huang, C., Lokugamage, K., Ikegami, T., Ito, N., Kubo, H., and
690 Makino, S. (2006). Severe acute respiratory syndrome coronavirus nsp1 protein suppresses host gene
691 expression by promoting host mRNA degradation. Proc. Natl. Acad. Sci. U. S. A.

692 Koepke, L., Winter, B., Grenzner, A., Regensburger, K., Engelhart, S., van der Merwe, J.A., Krebs,
693 S., Blum, H., Kirchhoff, F., and Sparrer, K.M.J. (2020). An improved method for high-throughput
694 quantification of autophagy in mammalian cells. Sci. Rep. *10*, 1–20.

695 Krüger, J., Groß, R., Conzelmann, C., Müller, J.A., Koepke, L., Sparrer, K.M.J., Schütz, D.,
696 Seufferlein, T., Barth, T.F.E., Stenger, S., et al. (2020). Remdesivir but not famotidine inhibits SARS-
697 CoV-2 replication in human pluripotent stem cell-derived intestinal organoids. BioRxiv
698 2020.06.10.144816.

699 Ksiazek, T.G., Erdman, D., Goldsmith, C.S., Zaki, S.R., Peret, T., Emery, S., Tong, S., Urbani, C.,
700 Comer, J.A., Lim, W., et al. (2003). A novel coronavirus associated with severe acute respiratory
701 syndrome. N. Engl. J. Med. *348*, 1953–1966.

702 Lam, T.T.Y., Shum, M.H.H., Zhu, H.C., Tong, Y.G., Ni, X.B., Liao, Y.S., Wei, W., Cheung,
703 W.Y.M., Li, W.J., Li, L.F., et al. (2020). Identifying SARS-CoV-2 related coronaviruses in Malayan
704 pangolins. Nature.

705 Lamers, M.M., Beumer, J., van der Vaart, J., Knoops, K., Puschhof, J., Breugem, T.I., Ravelli,
706 R.B.G., Paul van Schayck, J., Mykytyn, A.Z., Duimel, H.Q., et al. (2020). SARS-CoV-2 productively
707 infects human gut enterocytes. Science *369*, 50–54.

708 Letko, M., Marzi, A., and Munster, V. (2020). Functional assessment of cell entry and receptor usage
709 for SARS-CoV-2 and other lineage B betacoronaviruses. Nat. Microbiol. *5*, 562–569.

710 Li, K., Markosyan, R.M., Zheng, Y.M., Golfetto, O., Bungart, B., Li, M., Ding, S., He, Y., Liang, C.,
711 Lee, J.C., et al. (2013). IFITM Proteins Restrict Viral Membrane Hemifusion. PLoS Pathog. *9*.

712 Major, J., Crotta, S., Llorian, M., McCabe, T.M., Gad, H.H., Priestnall, S.L., Hartmann, R., and
713 Wack, A. (2020). Type I and III interferons disrupt lung epithelial repair during recovery from viral
714 infection. Science (80-.). eabc2061.

715 Mantlo, E., Bukreyeva, N., Maruyama, J., Paessler, S., and Huang, C. (2020). Antiviral activities of
716 type I interferons to SARS-CoV-2 infection. Antiviral Res. *179*, 104811.

717 Matsuyama, S., Nagata, N., Shirato, K., Kawase, M., Takeda, M., and Taguchi, F. (2010). Efficient
718 Activation of the Severe Acute Respiratory Syndrome Coronavirus Spike Protein by the
719 Transmembrane Protease TMPRSS2. J. Virol. *84*, 12658–12664.

720 Narayana, S.K., Helbig, K.J., McCartney, E.M., Eyre, N.S., Bull, R.A., Eltahla, A., Lloyd, A.R., and
721 Beard, M.R. (2015). The interferon-induced transmembrane proteins, IFITM1, IFITM2, and IFITM3
722 inhibit hepatitis C virus entry. J. Biol. Chem. *290*, 25946–25959.

723 Nchioua, R., Kmiec, D., Müller, J., Conzelmann, C., Groß, R., Swanson, C., Neil, S., Stenger, S.,
724 Sauter, D., Münch, J., et al. (2020). The Zinc Finger Antiviral Protein restricts SARS-CoV-2.
725 BioRxiv 2020.06.04.134379.

726 Perreira, J.M., Chin, C.R., Feeley, E.M., and Brass, A.L. (2013). IFITMs restrict the replication of
727 multiple pathogenic viruses. J. Mol. Biol. *425*, 4937–4955.

728 Pfaender, S., Mar, K.B., Michailidis, E., Kratzel, A., Hirt, D., V'kovski, P., Fan, W., Ebert, N.,
729 Stalder, H., Kleine-Weber, H., et al. (2020). LY6E impairs coronavirus fusion and confers immune
730 control of viral disease. BioRxiv Prepr. Serv. Biol. 2020.03.05.979260.

731 Rentsch, M.B., and Zimmer, G. (2011). A vesicular stomatitis virus replicon-based bioassay for the
732 rapid and sensitive determination of multi-species type I interferon. PLoS One.

733 Sa Ribero, M., Jouvenet, N., Dreux, M., and Nisole, S. (2020). Interplay between SARS-CoV-2 and

the type I interferon response. PLoS Pathog. *16*, e1008737.

Sallard, E., Lescure, F.X., Yazdanpanah, Y., Mentre, F., and Peiffer-Smadja, N. (2020). Type 1 interferons as a potential treatment against COVID-19. Antiviral Res. *178*, 104791.

Shi, G., Schwartz, O., and Compton, A.A. (2017). More than meets the I: The diverse antiviral and cellular functions of interferon-induced transmembrane proteins. Retrovirology *14*.

Shi, G., Kenney, A.D., Kudryashova, E., Zhang, L., Hall-Stoodley, L., Robinson, R.T., Kudryashov, D.S., Compton, A.A., and Yount, J.S. (2020). Opposing activities of IFITM proteins in SARS-CoV-2 infection. BioRxiv 2020.08.11.246678.

Smith, S.E., Weston, S., Kellam, P., and Marsh, M. (2014). IFITM proteins - Cellular inhibitors of viral entry. Curr. Opin. Virol. *4*, 71–77.

Sparrer, K.M.J., and Gack, M.U. (2015). Intracellular detection of viral nucleic acids. Curr. Opin. Microbiol. *26*, 1–9.

Volcic, M., Sparrer, K.M.J., Koepke, L., Hotter, D., Sauter, D., Stürzel, C.M., Scherer, M., Stamminger, T., Hofmann, T.G., Arhel, N.J., et al. (2020). Vpu modulates DNA repair to suppress innate sensing and hyper-integration of HIV-1. Nat. Microbiol.

Wrensch, F., Winkler, M., and Pöhlmann, S. (2014). IFITM proteins inhibit entry driven by the MERS-Coronavirus Spike protein: Evidence for Cholesterol-Independent Mechanisms. Viruses *6*, 3683–3698.

Yount, J.S., Moltedo, B., Yang, Y.Y., Charron, G., Moran, T.M., López, C.B., and Hang, H.C. (2010). Palmitoylome profiling reveals S-palmitoylation-dependent antiviral activity of IFITM3. Nat. Chem. Biol. *6*, 610–614.

Zang, R., Case, J.B., Castro, M.F.G., Liu, Z., Zeng, Q., Zhao, H., Son, J., Rothlauf, P.W., Hou, G.,

Bose, S., et al. (2020). Cholesterol 25-hydroxylase suppresses SARS-CoV-2 replication by blocking membrane fusion. BioRxiv 2020.06.08.141077.

Zani, A., and Yount, J.S. (2018). Antiviral Protection by IFITM3 In Vivo. Curr. Clin. Microbiol. Reports *5*, 229–237.

Zhao, X., Guo, F., Liu, F., Cuconati, A., Chang, J., Block, T.M., and Guo, J.T. (2014). Interferon induction of IFITM proteins promotes infection by human coronavirus OC43. Proc. Natl. Acad. Sci. U. S. A. *111*, 6756–6761.

Zhao, X., Sehgal, M., Hou, Z., Cheng, J., Shu, S., Wu, S., Guo, F., Le Marchand, S.J., Lin, H., Chang, J., et al. (2017). Identification of Residues Controlling Restriction versus Enhancing Activities of IFITM Proteins on Entry of Human Coronaviruses. J. Virol. *92*.

Zhao, X., Li, J., Winkler, C.A., An, P., and Guo, J.T. (2019). IFITM genes, variants, and their roles in the control and pathogenesis of viral infections. Front. Microbiol. *10*.

Zhao, X., Zheng, S., Chen, D., Zheng, M., Li, X., Li, G., Lin, H., Chang, J., Zeng, H., and Guo, J.-T. (2020). LY6E Restricts the Entry of Human Coronaviruses, Including the Currently Pandemic SARS-CoV-2. J. Virol.

Zhou, P., Yang, X. Lou, Wang, X.G., Hu, B., Zhang, L., Zhang, W., Si, H.R., Zhu, Y., Li, B., Huang, C.L., et al. (2020). A pneumonia outbreak associated with a new coronavirus of probable bat origin. Nature *579*, 270–273.

Figure 1

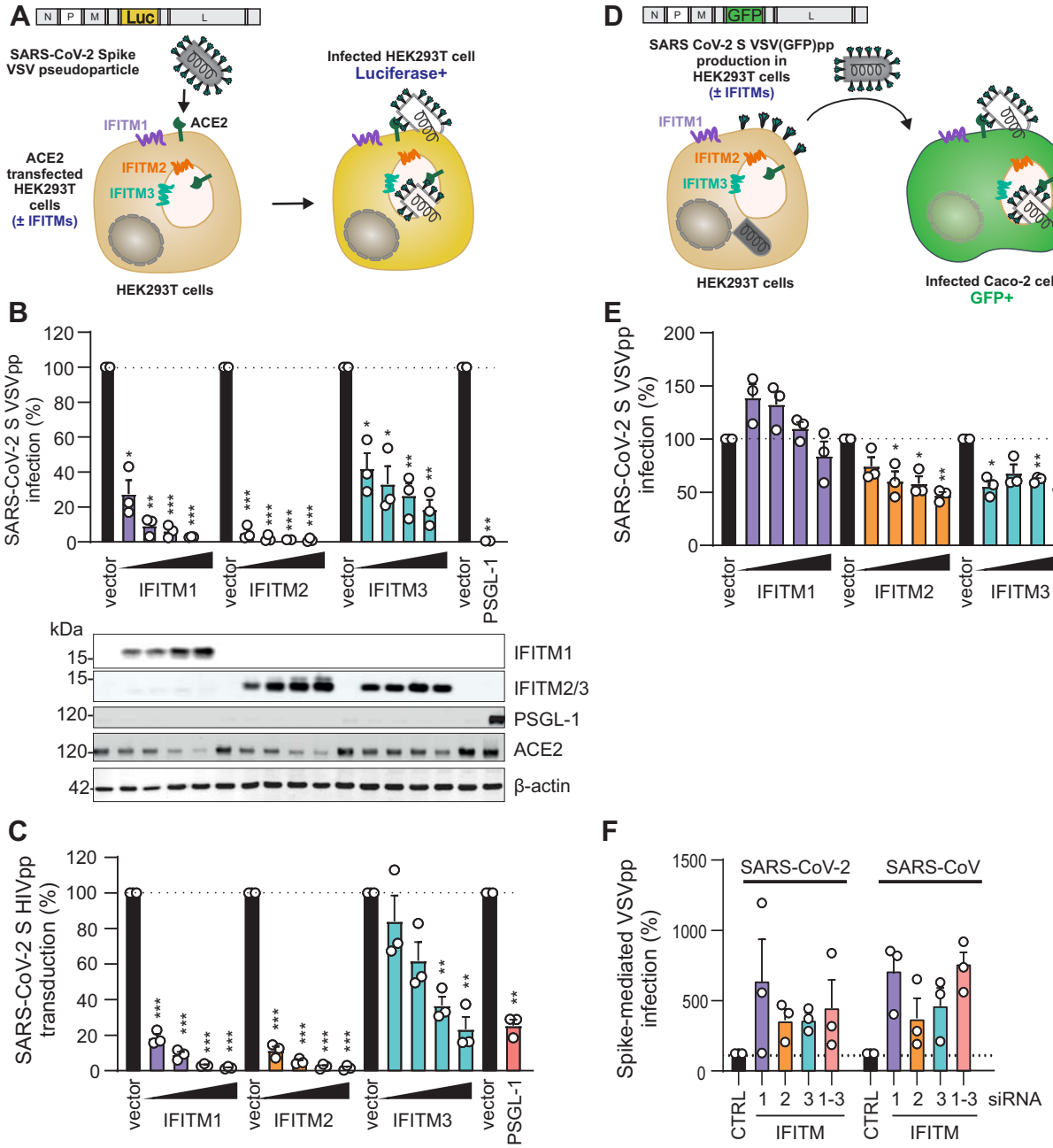

Figure 2

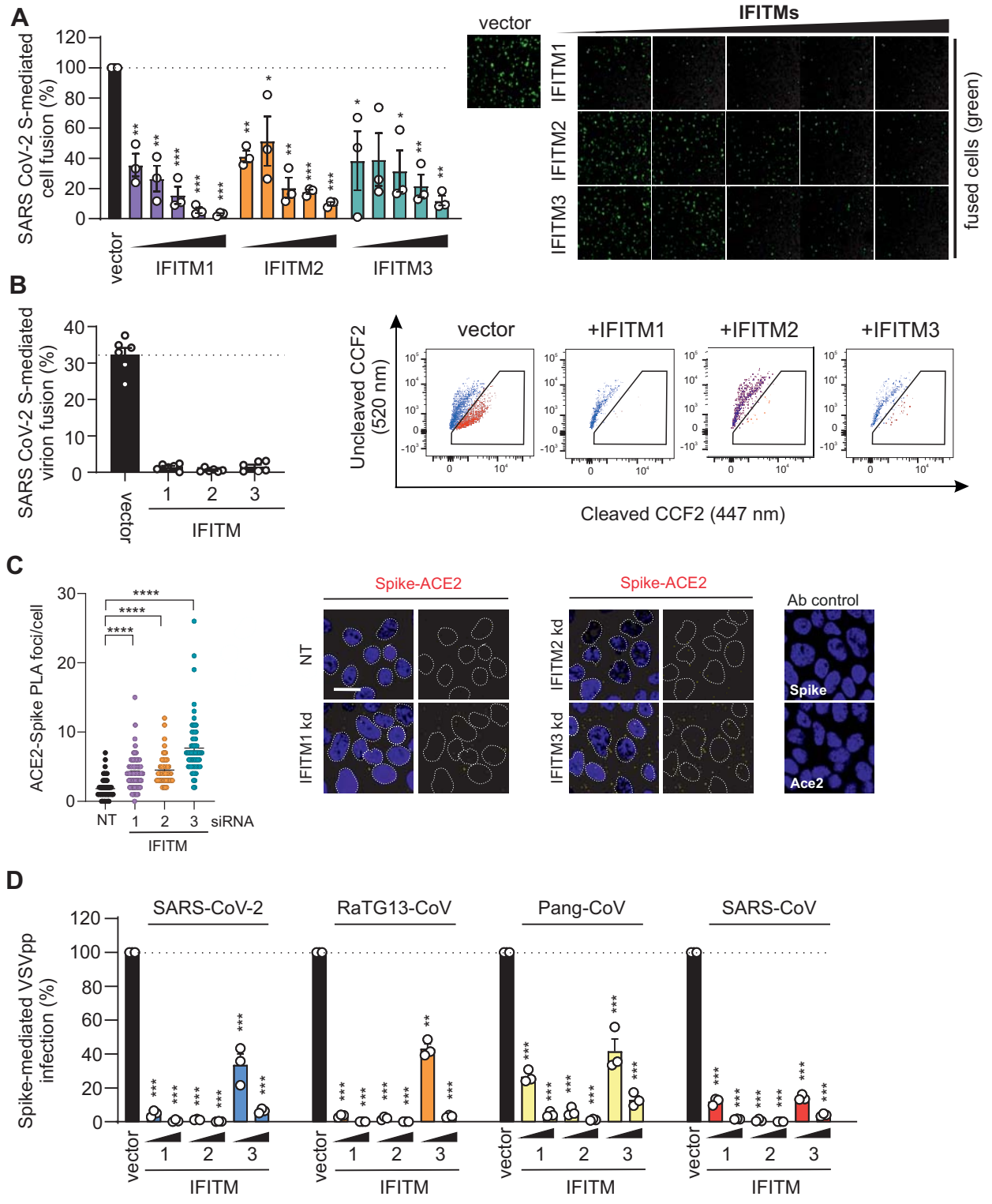

Figure 3

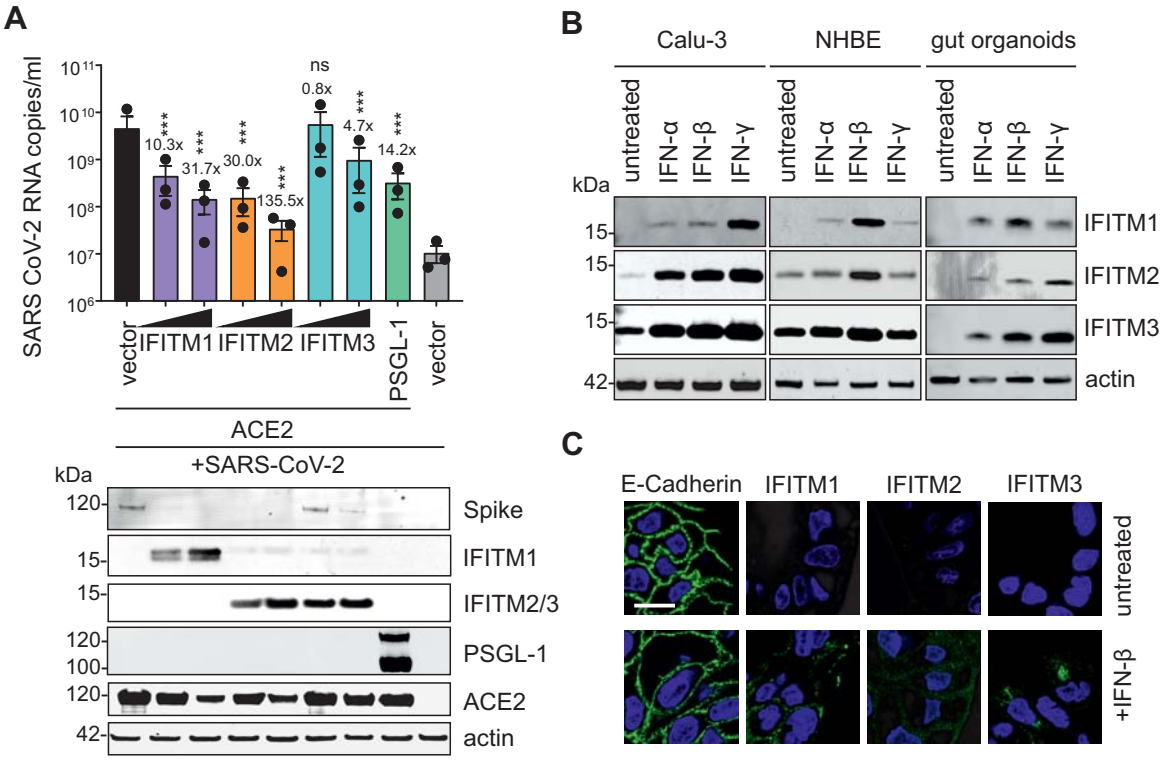

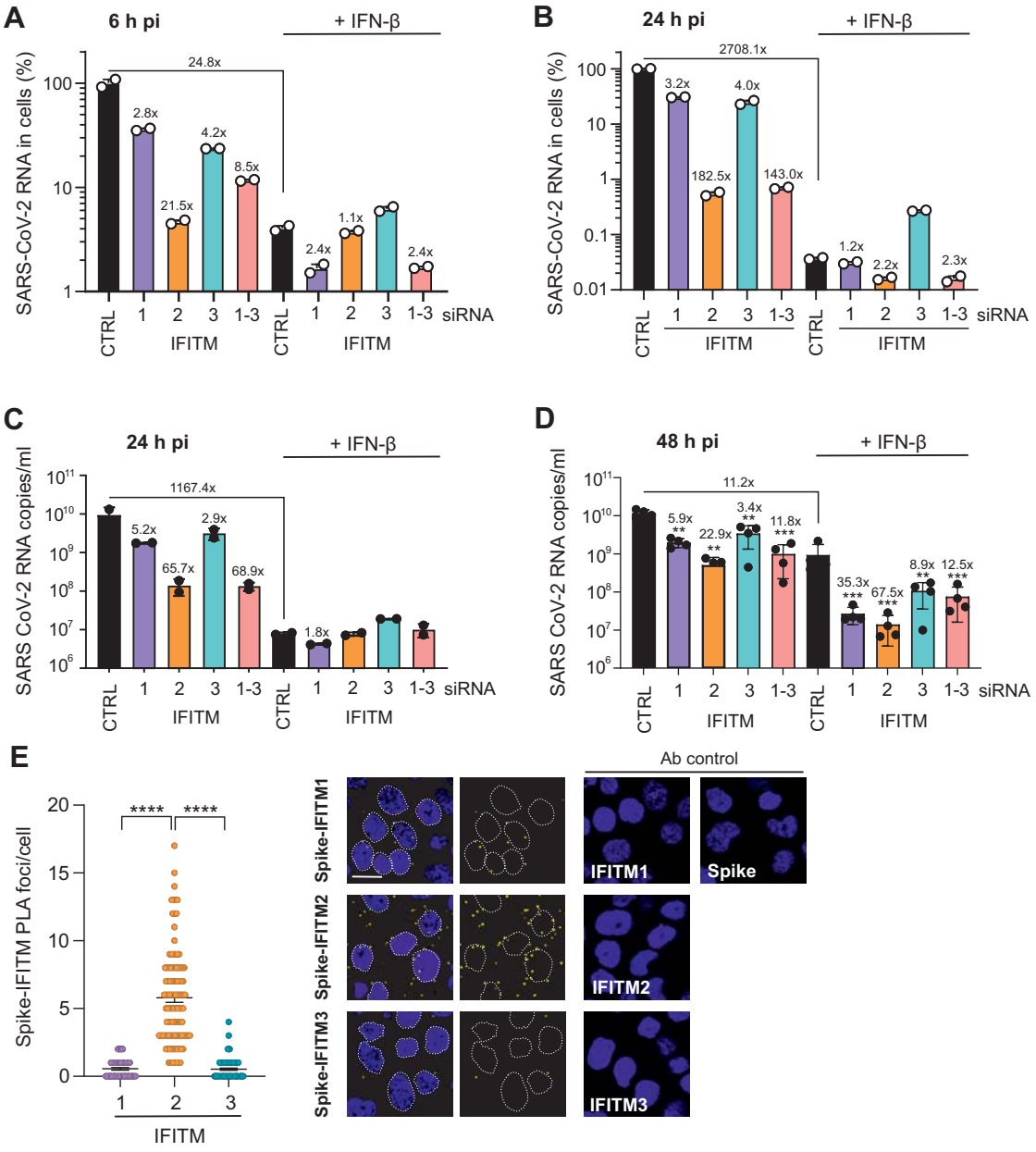

SUPPLEMENTAL FIGURES

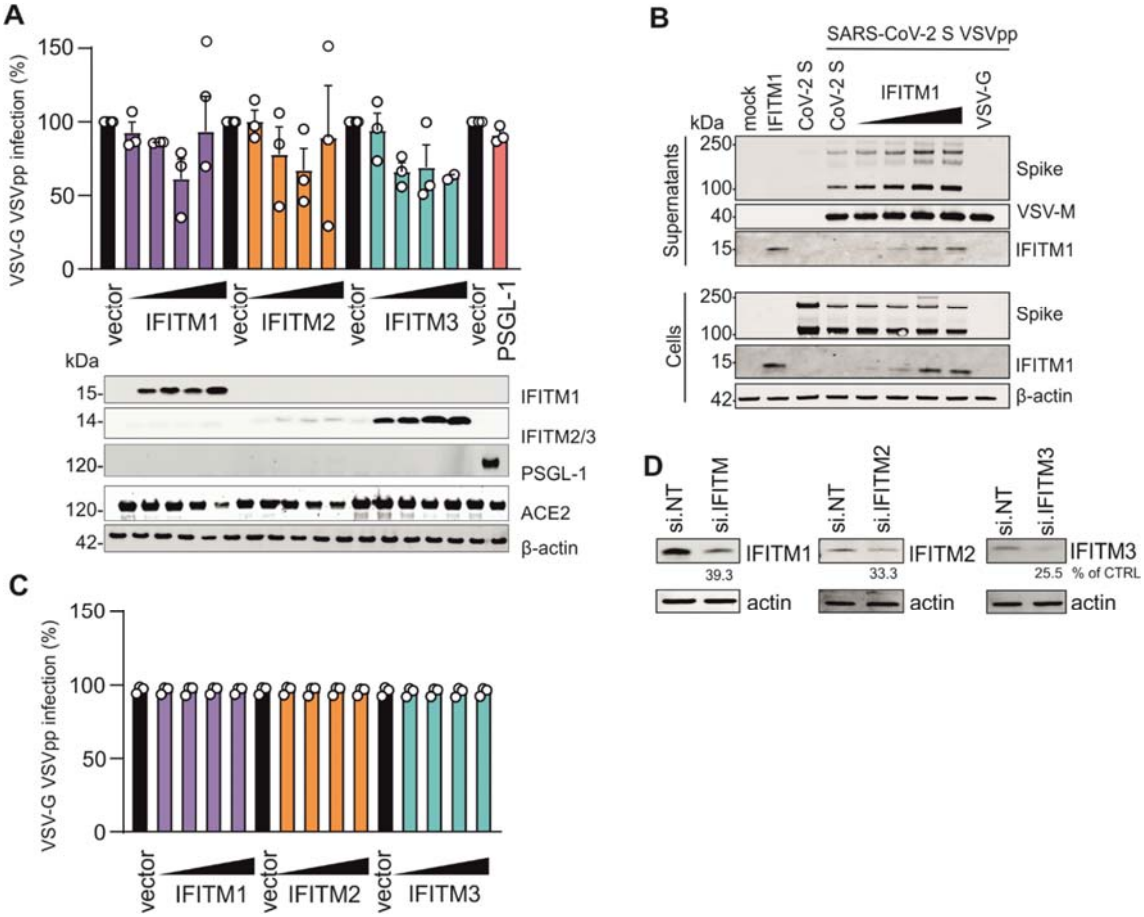

Figure S1 (related to Figure 1). VSV-G-mediated infection by VSVpp is not significantly inhibited by IFITM proteins.

(A) Quantification of VSV(luc)ΔG*VSV-G entry by luciferase activity in HEK293T cells transiently expressing indicated proteins and infected 24h post transfection with VSV(luc) ΔG*VSV-G (MOI 0.025) for 16 h. Bars represent means of n=3±SEM. Lower panel: Immunoblot of the corresponding whole cell lysates (WCLs) stained with anti-IFITM1, anti-IFITM2, anti-IFITM3, anti-PSGL-1, anti-ACE2 and anti-actin. (B) Immunoblot analysis of whole cell or supernatant lysates of HEK293T cells transiently transfected with SARS-CoV-2 S VSVpp and increasing doses of IFITM1 expression construct. Blots were stained with anti-Spike, anti-VSV-M, anti-IFITM1 and anti-actin. (C) Quantification of VSV(luc) ΔG*VSV-G particles by luciferase activity in Caco-2 cells infected with the supernatant from HEK293T cells transiently transfected with VSV-G and empty control or IFITM expression vectors. Bars represent means of n= 3±SEM. (D) Exemplary immunoblots of whole cell lysates of Calu-3 cells transiently transfected with control siRNA (si.NT) or siRNAs targeting IFITM1, 2 or 3 as indicated. Percentages indicate signal intensity of the three IFITM proteins relative to those observed in the presence of the control siRNA (100%).

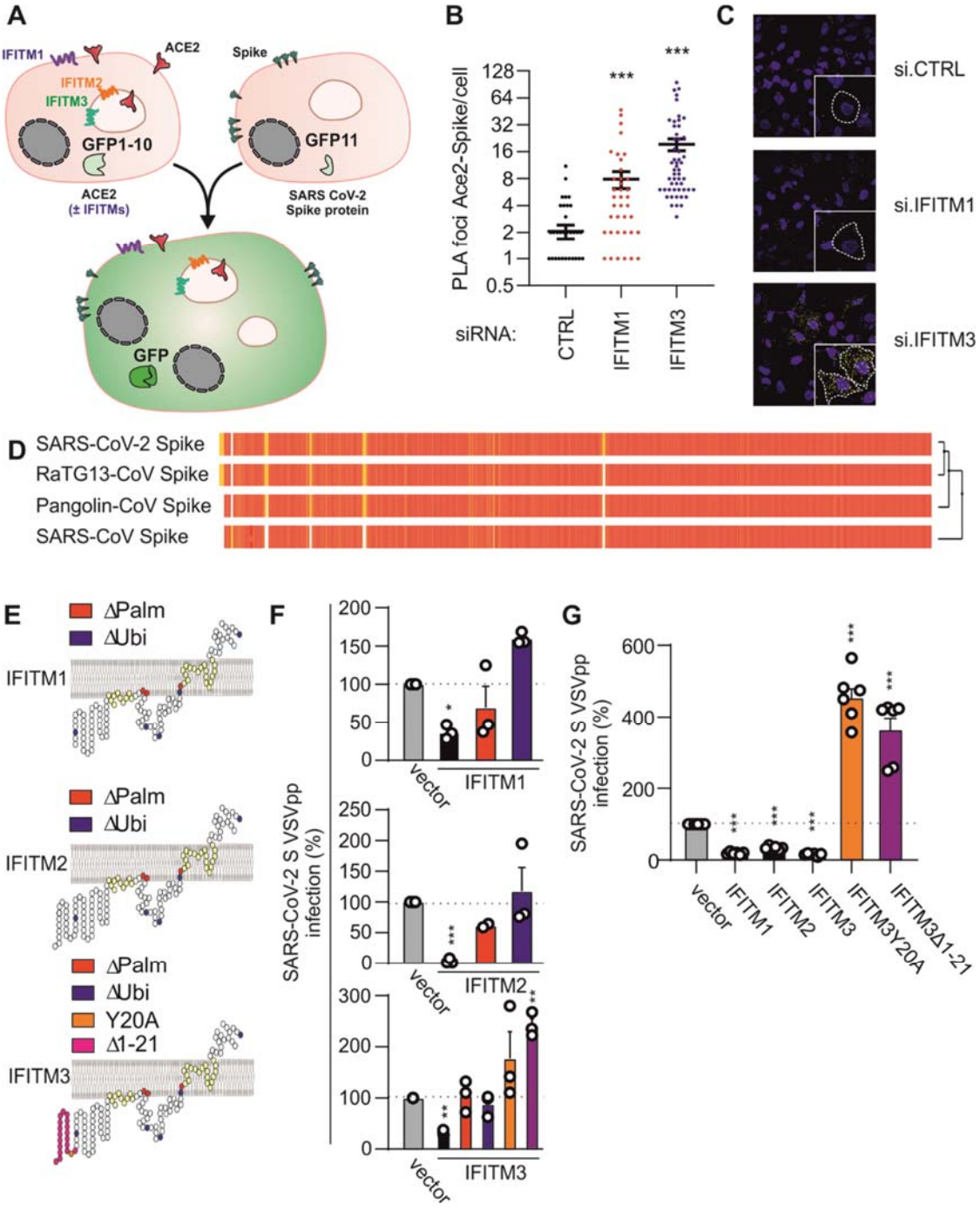

Figure S2 (related to Figure 2). Spectrum and determinants of the Spike-mediated fusion inhibition of IFITMs.

(A) Schematic depiction of the Split-GFP fusion assay. (B) Proximity ligation assay of ACE2 and SARS-CoV-2 Spike in HeLa cells. Cells were transfected with siRNA (CTRL, IFITM1 and IFITM3) and infected with VSV(luc)ΔG*SARS-CoV-2-S for 2 h at 4°C. Lines represent means of n=(77-84 cells)±SEM. (C) Exemplary images of the PLA assay shown in panel B. Spike-ACE2 PLA signal (red). Nuclei, DAPI (blue). The inset depicts a magnification, membrane outline of a cell depicted by a dotted white line. Scale bar, 20 µm. (D) Alignment of the Spike amino acid sequences from SARS-CoV-2, Pangolin-CoV, RaTG13-CoV and SARS-CoV. Yellow, low conservation; red, high conservation. Right panel: Neighbor-joining tree showing the phylogenetic relation of the sequences. (E) Schematic depiction of the three IFITM proteins in relation to the plasma membrane. Yellow, transmembrane parts. Alanine substitutions are color coded. Blue, Ubiquitination-negative mutant. Red, Palmitoylation negative mutant. Pink, Y20A. orange, NtΔ21AA20. (F) Quantification of the entry of VSV(luc)ΔG*-SARS-CoV-2-S by luciferase activity in HEK293T cells transiently expressing indicated proteins (IFITM mutants) and infected 24 h post-transfection with the VSVpp (MOI 0.025) for 16 h. Bars represent means of n=3±SEM. (G) Quantification of the entry of HIV(Fluc)Δenv*-SARS-CoV-2-S by luciferase activity in HEK293T cells stably expressing indicated proteins (IFITM mutants) and ACE2. The cells were transduced with the HIVpp for 48h. Bars represent means of n=6±SEM.

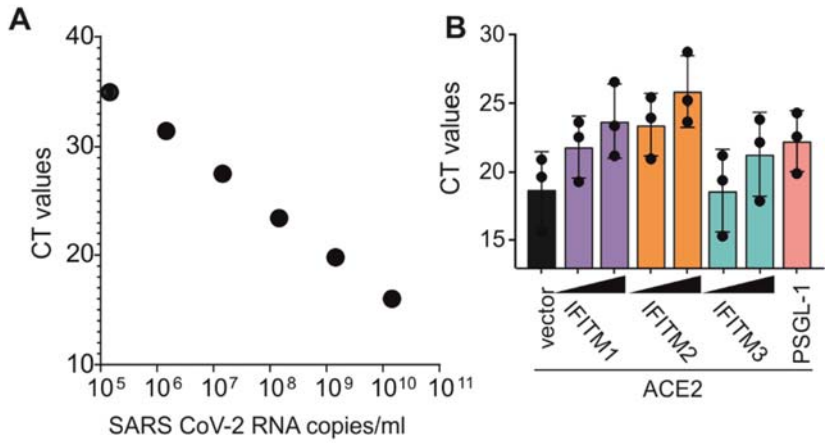

Figure S3 (related to Figure 3). Quantification of SARS-CoV-2 N gene RNA by qRT-PCR in the supernatant of virally infected HEK293T cells.

Standard curve (left) and raw qRT-PCR CT values (right) corresponding to the SARS-CoV-2 RNA copy numbers per ml shown in Figure panel A. The bar diagram shows mean raw qRT-PCR (+/- SD) from three replicates.

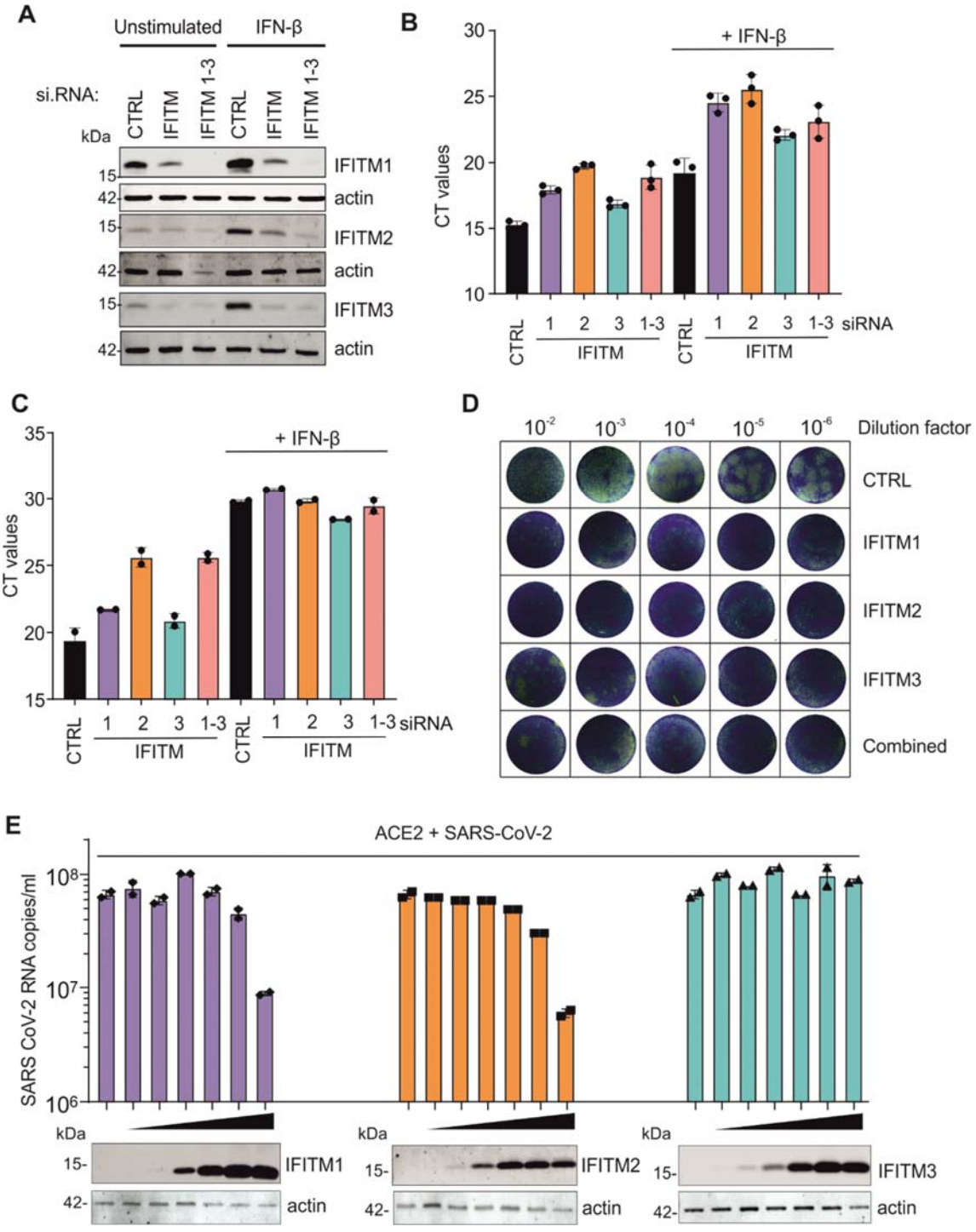

Figure S4 (related to Figure 2). Impact of endogenous and transient IFIM expression on SARS-CoV-2 replication.

(A) Exemplary immunoblots of whole cell lysates of Calu-3 cells transiently transfected with siRNA either control (si.NT) or targeting IFITM1, 2 3 (si.IFITM1, 2, 3) as indicated. (B, C) Raw Ct values of the viral N gene RNA levels shown in Figure 4 panel C and D. (D) CPE (white) after 72h caused by infection of monolayers of Vero cells with serial dilutions of Calu-3 supernatants form Figure 4D. Cells were stained with crystal violet (blue). (E) SARS-CoV-2 RNA production from HEK239T cells transient expressing ACE2 and increasing levels of the indicated IFITM proteins. Quantification of viral N gene RNA by qRT-PCR in the supernatant of HEK293T was performed 48 h post-infection with SARS-CoV-2 (MOI 0.05). Bars represent means of n=2±SEM.